Atmospheric Pollution Research 17 (2026) 102746

Contents lists available at ScienceDirect

Atmospheric Pollution Research

journal homepage: www.elsevier.com/locate/apr

First long-term air quality assessment in Luanda, Angola: Performance evaluation of a low-cost monitoring station against reference equipment

Alan Victor da Silva [a,*], Leonardo Furst [a], Yago A. Cipoli [a], Marlene J.S. Soares [a], Anabela G.A. Leitão [b], Manuel Feliciano [c], Célia A. Alves [a,**]

[a] Department of Environment and Planning, CESAM — Centre for Environmental and Marine Studies, University of Aveiro, 3810-193, Aveiro, Portugal
[b] LESRA – Separation, Chemical Reaction, and Environmental Engineering Laboratory, Agostinho Neto University, Luanda, Angola
[c] CIMO — Mountain Research Centre, LA SusTEC — Associated Laboratory for Sustainability and Technology in Inland Regions, Polytechnic Institute of Bragança, Campus de Santa Apolónia, 5300-253, Bragança, Portugal

ARTICLE INFO

Keywords:
Low-cost sensors
Optical methods
Beta attenuation monitor
Gravimetric methods
Luanda

ABSTRACT

Low-cost air quality monitoring stations (LCMS), which integrate sensors for gases and particulate matter (PM), offer an economical solution for expanding monitoring networks. However, their reliability requires validation, particularly in rapidly urbanising regions with limited infrastructure. This study presents the first long-term, continuous, multi-pollutant air quality assessment in Luanda, Angola - where no monitoring stations currently exist - by evaluating the performance of an LCMS against reference-grade equipment. Daily averages, correlation metrics (R^2, RMSE), and a hybrid Bland-Altman/regression analyses were used to evaluate the agreement. Results indicated strong correlation for CO ($R^2 = 0.96$; RMSE = 0.24 ppm) and good for NO_2 ($R^2 = 0.81$; RMSE = 6.35 ppb), although limitations near detection limits were noted. Significant challenges were identified in O_3 measurements ($R^2 = 0.77$, RMSE = 7.13 ppb), primarily due to strong cross-sensitivity to high ambient NO_2 levels and potential sensor ageing. For PM_{10} and $PM_{2.5}$, although good linear correlations ($R^2 \sim 0.82$) were observed with reference methods, the LCMS exhibited considerable systematic bias (RMSE over 46 $\mu g/m^{-3}$) and consistently underestimate concentrations. The study also registered frequent and severe exceedances of WHO AQG and EU standards for PM_{10}, $PM_{2.5}$, and NO_2, underscoring significant public health risks. Despite limitations, particularly for O_3 measurements and biases in PM data, the LCMS demonstrates potential as a cost-effective tool to complement reference networks, enhance spatial monitoring coverage, identify pollution hotspots, and support air quality management in resource-constrained settings, since continuous calibration and validation procedures are implemented to mitigate measurement uncertainties.

1. Introduction

Air pollution is increasingly recognised as a critical global health challenge and is currently ranked as the second-leading risk factor for premature deaths worldwide. Despite advances in medicine and the rise in life expectancy, air pollution remains responsible for approximately one in every eight deaths globally (Health Effects Institute, 2024). Its contribution to the global burden of cardiovascular and respiratory diseases is largely driven by its role in the aggravation of chronic conditions (Koehler et al., 2018; Rosenthal, 2015). In response to the growing body of evidence linking exposure to pollutants - such as nitrogen oxides (NOx), carbon monoxide (CO), ozone (O_3), and particulate matter (PM) - with adverse health outcomes, international organisations have established comprehensive air quality standards (Alvarez et al., 2020; Cushing et al., 2015; Lee et al., 2021). These include the European Air Quality Directive 2024/2881 (EU, 2024), the World Health Organisation Air Quality Guidelines (WHO, 2021), and the United States Environmental Protection Agency Ambient Air Quality Standards (U.S. EPA, 2014). However, the effectiveness and enforcement of these guidelines or standards remain uneven across the globe, especially in rapid urbanising regions, such as Africa (Fisher et al., 2021).

Urban air pollution primarily originates from mobile, stationary, and area sources, which significantly contribute to levels of PM less than 10 and 2.5 μm (PM_{10} and $PM_{2.5}$), as well as gaseous pollutants

* Corresponding author.
** Corresponding author.
E-mail addresses: alansilva@ua.pt, alanvisi@gmail.com (A.V. da Silva), celia.alves@ua.pt (C.A. Alves).

https://doi.org/10.1016/j.apr.2025.102746
Received 27 May 2025; Received in revised form 9 September 2025; Accepted 9 September 2025
Available online 12 September 2025

(Aggoune-Mtalaa and Laib, 2023; Lelieveld et al., 2015; Simwela et al., 2018). These pollution sources not only affect local air quality but also exacerbate transboundary pollution, raising concerns about the broader environmental impacts of megacities (Bikkina et al., 2019; Cassiani et al., 2013; Mishra and Kulshrestha, 2021; Yoshino et al., 2021). Rapid population growth and urbanisation have led to a 60% increase in outdoor air pollution-related deaths in Africa from 1990 to 2017 (Rees et al., 2019). The continent experienced an estimated 1.1 million deaths from air pollution in 2019, with household air pollution and ambient $PM_{2.5}$ being major contributors, with 697,000 (95%: UI 526,000–879,000) and 383,000 deaths (95% UI: 289,000–491,000), respectively (Fisher et al., 2021). Comparatively, premature deaths from air pollution are twice as high in Africa as in Europe (Kebede et al., 2021; Niemenmaa et al., 2018; Shikwambana and Tsoeleng, 2020). Only 6% of African children live near reliable air quality monitoring stations, a stark contrast to the 72% in Europe and North America (Rees et al., 2019). As of 2020, only 11 out of 54 African countries had any reliable, real-time air pollution monitoring network. This means that in most African cities, pollution levels are an unknown threat, silently affecting the health of populations, especially the most vulnerable (Fuller et al., 2022; Health Effects Institute, 2024; IQAir, 2020). Improved data would inform evidence-based policies to protect the health of over half a billion African children who are currently underserved and undercounted (Pinder et al., 2019; Rees et al., 2019). Satellite-based models help estimate pollution levels (Atuhaire et al., 2022; Malings et al., 2020; Munyaradzi Makoni, 2020; Zhang et al., 2021), but without local calibration from ground stations, these satellite-derived estimates can carry large uncertainties, ranging from 22% to 85% (Bai et al., 2019; Fuller et al., 2022; Ma et al., 2014; Seltenrich, 2017). Therefore, accurate and reliable ground-level monitoring devices remain primordial for assessing exposure and formulating effective pollution control policies (Bauer et al., 2019; Simwela et al., 2018).

Reference-grade monitoring equipment is known for its accuracy, although with drawbacks such as high costs, complexity, and logistical challenges. Low-cost sensors typically use technologies such as electrochemical cells and optical particle counters, offering affordable air quality monitoring solutions, with costs ranging from $10 to $100 each (Chojer et al., 2020; Giordano et al., 2021). The advent of these devices for air quality monitoring offers an economical solution for spatial analysis and real-time data acquisition, though their reliability compared to reference-grade equipment remains a critical area for investigation (Hua et al., 2021). Their performance can be affected by environmental factors such as temperature, humidity, and the presence of other airborne chemicals (Clements et al., 2019; Giordano et al., 2021; Kelly et al., 2017; Zusman et al., 2020). Therefore, the need for calibration and susceptibility to environmental factors must be carefully considered when deploying these devices for air quality assessment. (Badura et al., 2018; di Meane et al., 2009; Kiss et al., 2017; Kovacs et al., 2021; Triantafyllou et al., 2016).

The primary aim of this study is to conduct a temporal analysis of ground-level air quality in Luanda, Angola, a rapidly developing urban area, by measuring meteorological parameters alongside key air pollutants (CO, O_3, NOx, and size-distributed particulate matter). Concurrently, this research evaluates the performance of a low-cost air quality monitoring station (LCMS) as a viable, real-time, and cost-effective solution for monitoring in regions with limited infrastructure. By simultaneously addressing gases and particulate matter and applying advanced calibration techniques, this study fills a clear gap in the literature and provides evidence directly relevant to regions lacking formal monitoring networks. It represents the first long-term, continuous, multi-pollutant assessment of air quality in Luanda, and one of the very few conducted in sub-Saharan Africa (Amegah et al., 2018; Atuyambe et al., 2024; Gualtieri et al., 2024; Raheja et al., 2023; Subramanian et al., 2024). This exploratory research is crucial for expanding scientific monitoring data, informing public health policies, supporting regulatory frameworks, and enabling early warning systems in regions where conventional monitoring remains scarce and low-cost sensors are being considered.

2. Material and methods

2.1. Instrumentation

The Bettair® Static Nodes MK2.5 (BET00210085) is a LCMS that directly transmits data to a cloud server and guarantees data integrity for up to two years. It is equipped with electrochemical gas sensors designed to detect pollutants such as NOx, CO, O_3, and SO_2, presenting their concentrations in parts per billion (ppb) or micrograms per cubic meter ($\mu g\ m^{-3}$). Additionally, it integrates an Optical Particle Counter (OPC) for measuring particulate matter smaller than 10, 2.5 or 1 μm (PM_{10}, $PM_{2.5}$, and PM_1, respectively), along with sensors for temperature, relative humidity, and atmospheric pressure. Furthermore, the device integrates algorithms that compensate for sensor ageing and variability.

The HORIBA® AP-Series gas analysers included: i) the APOA-360 & APOA-370 models for ozone (O_3) measurement, utilising non-dispersive ultraviolet absorption (UV Ref.Eq.; limit of detection: 0.5 ppb (3σ); repeatability: ±1.0%) technology, ii) the APMA-370 model, designed for carbon monoxide (CO) measurement, employing non-dispersive infrared (IR Ref.Eq.; limit of detection: 0.02 ppm (3σ); repeatability: ±1.0%) with cross-flow modulation, and iii) the APNA-370 model for nitrogen oxides (NO, NO_2, NOx), using reduced pressure chemiluminescence (CL Ref.Eq.; limit of detection: 0.5 ppb (3σ); repeatability: ±1.0 %). These analysers maintain consistent flow rates of 0.7, 0.8, and 1.5 L per minute for the APOA, APNA, and APMA, respectively, and all operate within an ambient temperature range of 5–40 °C. They are known for their precision in parts per billion (ppb) for the APOA and APNA, and in parts per million (ppm) for the APMA.

The DustTrak DRX 8533 (OM Eq.) is an instrument manufactured by TSI® based on an optical method (OM), capable of counting and sizing particles within the optical diameter range of 0.3–10 μm. It has a detection limit of 1 $\mu g\ m^{-3}$ and an accuracy of ±10%, operating effectively under temperatures between 0 and 50 °C and relative humidity from 0 to 95% (non-condensing). The DustTrak aerosol monitor typically uses a default particle density value of 1 g/cm^3 (Arizona test dust), which is provided by the manufacturer.

The Beta monitor F-701-20 (BM Eq.; limit of detection: 1 $\mu g\ m^{-3}$; accuracy: 8.5%; operational temperature and humidity: 0–40 °C and 0–100% RH (non-condensing)), developed by DURAG®, stands as an advanced instrument designed for the continuous monitoring of atmospheric particulate matter less than 2.5 or 10 μm. It operates on the principle of extractive radiometric measurement, utilising Beta radiation attenuation methods (BM) to accurately and efficiently gauge particulate matter levels in the atmosphere. In addition, this equipment includes an internal heating system that prevents humidity from affecting the measurements.

The TECORA® Echo PM (GM $Ref.Eq_1$.) and AMS® high volume sampler (GM $Ref.Eq_2$.) are employed for sampling and determining PM concentrations using gravimetric methods (GM). These methods involve weighing the filters both before and after sampling, in accordance with the European Norm 12341:2023 (CEN, 2023). Sampling was carried out for 23 h and 30 min, starting daily at 06:00 a.m. (local time). After sampling, filters were frozen at −18 °C until further processing to preserve their integrity. The weighing process took place in a room with controlled humidity (50%) and temperature (20 °C) to ensure stability and accuracy. This procedure was repeated for each sample multiple times until a standard deviation less than 2% was obtained between values of at least 6 weightings. Due to occasional power outages in Luanda, some sampling durations were shorter. Only gravimetric data from samples representing more than 75% of the 24-h period were included in the analysis.

The meteorological station (MS) was equipped with a comprehensive

set of devices for monitoring various weather parameters. It included a CS215 sensor for measuring temperature and relative humidity, a PYR-S pyranometer for solar radiation (SR), and an ARG100 rain gauge for precipitation measurement. Additionally, the station incorporated a cup anemometer for wind speed (WS) and a wind vane for wind direction.

2.2. Monitoring site and experimental design

From June 27, 2023, to November 05, 2023, the monitoring devices were installed at the Faculty of Engineering, Agostinho Neto University, located in the heart of Luanda, the capital of Angola, on the west coast of Africa (−8°50′49.77″ S, 13°13′51.11″ W). According to data from 2022, more than 9 million inhabitants live in the metropolitan area of Luanda. It is the most densely populated area in Angola, accounting for 1/3 of the nations' total population. It experiences a humid tropical climate with average daily temperatures above 29 °C during summer months and slightly cooler conditions below 27 °C in winter. The city's climate is marked by two distinct seasons: a rainy season from August to May and a dry season from May to August, known as cacimbo season (Campos et al., 2021).

In Luanda, air pollution is a pressing issue driven by rapid urbanisation and industrial growth. One of the primary sources of air pollution is vehicle emissions, as the number of cars, trucks, and buses on the roads has significantly increased, many of which are older models with less stringent emission controls. This surge in traffic leads to the release of pollutants such as nitrogen oxides (NOx), carbon monoxide (CO), and particulate matter (PM). Additionally, industrial activities, including oil refining and manufacturing, contribute to poor air quality, emitting volatile organic compounds (VOCs), sulphur dioxide (SO_2), and other harmful substances. To ensure minimal distance between sampling inlets and thus enhance the accuracy of data collection, the equipment was meticulously arranged side-by-side (Fig. 1 B). The LCMS was co-located with the meteorological station, all available Horiba AP-370 Series for gases, and a Beta attenuation monitor for $PM_{2.5}$. In addition, two gravimetric samplers equipped with PM_{10} inlets were used: a high-volume sampler equipped with 15 cm quartz filters from Pall, and a low volume sampler equipped with 47 mm Teflon filters, also from Pall. Quartz filters were previously baked at 500 °C to eliminate organic contaminants. For intercomparison purposes, two other instruments were used for particle monitoring for shorter periods: a DustTrak (continuous measurement of PM_{10}, $PM_{2.5}$ and PM_1 by photometry) for 23 days, and a low volume sampler from TECORA equipped with 47 mm quartz filters and a $PM_{2.5}$ inlet for 11 days. Table S1 provides an overview of the monitoring campaigns, detailing the monitoring periods and equipment used. Before the monitoring campaigns, all devices underwent factory calibration to ensure the precision and reliability of measurements, except for the LCMS, which was made available on October 1, 2021, and had not been calibrated for approximately 1.74 years by the start of the campaign.

2.3. Data processing

Data were acquired in local time (LT) and, to align with PM collection time by gravimetric samplers, all daily averages represent the period between 06:00 a.m. of one day and 06:00 a.m. of the next day, following the provisions of the 2011/850/EU Directive (EC, 2011). The dataset was organised in an Excel spreadsheet for accessibility and processed with Python coding language using libraries like NumPy, MatPlotLib, Sklearn, and Pandas for graphical analysis and statistical evaluation. This included the creation of average daily profiles from hourly measurements and linear correlation analyses between equipment measuring the same parameters. Additionally, a hybrid plot combining elements of Bland-Altman and linear regression was used. This plot shows the regression line along with the limits of agreement,

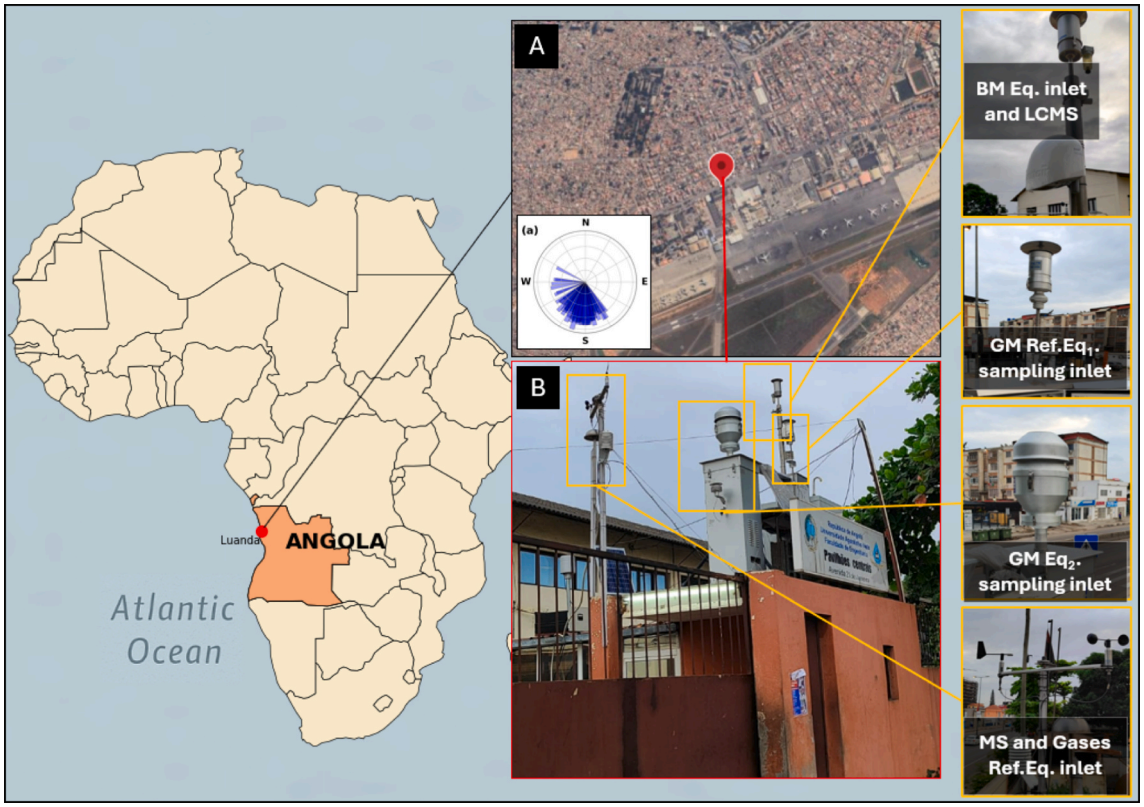

Fig. 1. Study site location in Luanda, Angola, with satellite imagery (A) and wind rose diagram indicating wind origin and frequency throughout the campaign (a); Equipment setup used (B) for the intercomparisons. LCMS – Low-cost monitor station; MS – meteorological station, Gases Ref. Eq. – Gas analysers, Horiba, AP-370 Series; BM Eq. – Beta monitor; GM Ref. Eq_1. – Low-volume sampler; GM Ref. Eq_2. – High-volume sampler. Satellite imagery from Google Earth (accessed April 2025).

which are defined as the mean difference between measurements ±1.96 standard deviations (SD). The shaded area represents the concordant measurements, with the midline indicating the expected correlation between the methods. Subsequently, key parametric metrics were calculated, such as R^2 and Root Mean Square Error (RMSE).

For each hourly measurement, an additional column named 'Measurement Difference' was added to the dataset, representing the absolute difference between the readings from LCMS and the reference equipment. To investigate the impact of environmental variables on these measurement discrepancies, the Spearman's rank correlation coefficient (ρ) was used, as it assumes non-parametric relation between measurement difference (LCMS vs. Ref.Eq.) and the environmental parameter. This analysis revealed the degree to which environmental factors influence the discrepancies in the readings. A threshold of $|\rho| \geq 0.4$ was adopted to identify relevant predictors, and statistical significance was established at p-value<0.05. Through this analysis, it was possible to observe and investigate potential systematic bias errors of the LCMS compared to the reference equipment and their possible environmental causes.

Furthermore, Spearman's correlation was employed as a conditional parameter to guide variable selection for multiple linear regression (MLR). Subsequently, to address multicollinearity, a multi-stage filter strategy was applied: (i) within highly correlated variable families (e.g., NOx or PM), only the variable with the strongest absolute correlation to the measurement error was retained; (ii) if the target LCMS variable belonged to one of these families, no other variables from the same family were included (iii) redundant duplicates (e.g., LCMS vs. reference forms of the same pollutant); were removed; (iv) residual multicollinearity was addressed by calculating the variance inflation factor (VIF), with iterative removal of variables exceeding a threshold of 10, while always retaining the LCMS target variable. This procedure was performed separately for LCMS-based auxiliary variables (LCMS) and reference-based variables (Ref.). This multi-stage methodology was designed to ensure that the calibration models minimise overfitting while enhancing transferability across some environmental conditions (deSouza et al., 2022; O'Brien, 2007; Tamura et al., 2018). After selecting variables under these conditions, MLR was applied to develop an alternative statistical model capable of more accurately predicting LCMS measurements using relevant variables from the LCMS data.

A feed-forward artificial neural network (NN-MLP; multi-layer perceptron) was implemented using the same predictor selection as for the MLR-Ref., extending the analysis beyond the linear framework across the entire measurement campaign. All predictors were standardised (zero mean, unit variance) before fitting. The NN-MLP employed rectified linear unit (ReLU) activation, a linear output, L2 weight regularisation and early stopping. The network architecture and regularisation strength were adapted to the number of available samples: for very small datasets ($n < 80$), a compact single hidden layer (16 neurons) was used with stronger penalisation ($\alpha = 10^{-2}$) and increased validation fraction (30%) for early stopping; for intermediate datasets ($80 \leq n < 150$), a two-layer configuration (16 and 8 neurons) with moderate regularisation ($\alpha \approx 3 \times 10^{-3}$) and 25% validation was applied; for larger datasets ($n \geq 150$), a deeper network (32 and 16 neurons) with weaker regularisation ($\alpha = 10^{-3}$) and 20% validation was used. Early stopping with patience between 50 and 80 iterations (depending on n) was applied to mitigate overfitting. Model performance was assessed using the same metrics (R^2 and RMSE), with the NN-MLP providing a non-linear benchmark for comparison. The MLR models were implemented using the Linear Regression module from scikit-learn, VIF was calculated with statsmodels, and the NN-MLP was implemented in scikit-learn with a maximum of 5000 iterations and the Adam optimiser. Further details of the statistical formulas and calibration equations are provided in the Supplementary Materials (Section S1 and Fig. S1).

3. Results and discussion

3.1. Meteorological conditions

Graphical representations of meteorological data are available in the Supplementary Material (Fig. S3). Luanda's weather was characterised by solar radiation at 134 ± 134 W m^{-2} and temperatures averaging 23.7 ± 2.41 °C. Relative humidity remained stable at 80.7 ± 8.33%, and atmospheric pressure showed minor fluctuations, averaging 1008 ± 2.37 mbar. Wind speed averaged 1.51 ± 0.47 m s^{-1}, peaking between 14:00–17:00, mostly from the south-west. The period was generally dry, but significant rainfall was recorded on 10-24-2023 and 11-01-2023, exceeding 6 mm h^{-1}.

Comparison of hourly data from the meteorological station and the LCMS (Figs. S4 and S5) revealed strong correlations, with R^2 values of 0.94 and 0.98 for 1-h and 24-h temperature, and 0.92 and 0.87 for 1-h and 24-h relative humidity, respectively. Low RMSEs were observed (1.35 °C for temperature; 2.37% for humidity), suggesting good agreement. Averaging LCMS data to daily values improved agreement with reference measurements. The discrepancy in hourly temperature readings was more strongly correlated with WS ($\rho = -0.49$), suggesting increased variability under higher wind conditions. For relative humidity, measurement accuracy improved at higher humidity levels. Additionally, moderate correlations were observed between discrepancy in RH measurements and WS ($\rho = -0.60$) and temperature ($\rho = -0.41$).

3.2. Gaseous pollutants

3.2.1. Carbon monoxide (CO)

Measurements from the LCMS and IR reference equipment showed consistent agreement over both long-term (Fig. 2) and intraday periods (Fig. 3). Despite statistical differences, the scalar measurements over time were similar and exhibited good agreement between instruments, as shown in Fig. 4 (a) and (b) ($R^2 = 0.96$, RMSE = 0.24 ppm). Fig. 3 (a) shows that the largest discrepancies in CO measurements occurred primarily between 08:00 and 16:00, while the smallest were between 18:00 and 19:00 (average 0.045 ppm). These discrepancies were most strongly correlated with SR ($\rho = 0.49$), PM of all size fractions (average $\rho = 0.46$), and notably with NO concentrations (average $\rho = 0.55$), all of which likely contributed to systematic measurement bias. Conversely, RH exhibited a negative correlation ($\rho = -0.45$), suggesting improved measurement reliability under higher humidity conditions. These findings indicate that the LCMS showed reduced precision during periods of heightened daytime activity, when atmospheric gas reactions intensify, and CO concentrations increase. In contrast, reliability gradually improved at night, as RH levels increased.

Both the LMCS and IR Ref.Eq. recorded similar temporal variations, with CO concentrations of 0.74 ± 0.73 ppm and 0.90 ± 0.76 ppm, respectively. These values are comparable to those observed in São Paulo, Brazil, during the winter months from 2018 to 2021 (0.80 ± 0.45 ppm; Moreira et al., 2023) and Beijing (~1.04 ppm; Li et al., 2018; Liu et al., 2018). They are also in line with recent measurements in Mexico City (~0.67 ± 0.03 ppm; Díaz-Álvarez and de la Barrera, 2020). However, higher CO concentrations were reported in New Delhi (2.3 ± 0.6; Tyagi et al., 2016). Despite these moderate averages, peak values recorded (LMCS = 3.80 ppm, IR Ref.Eq. = 4.2 ppm) on 19 July 2023 at 08:00 indicate potential local episodes of CO accumulation, particularly during the dry season. The magnitude of this peak is comparable to rush hour levels observed in the São Paulo's metropolitan region in winter (up to 2.2 ppm; Rozante et al., 2017) and to daily maximum values reported in New Delhi. While both devices captured the peak value simultaneously, this synchronicity was not observed for the minimum values, which appeared to be more affected by local microclimatic conditions or variability in emissions. CO levels were generally stable throughout the monitoring period, showing only a slight decreasing trend and suggesting small, but significant, seasonal emission changes.

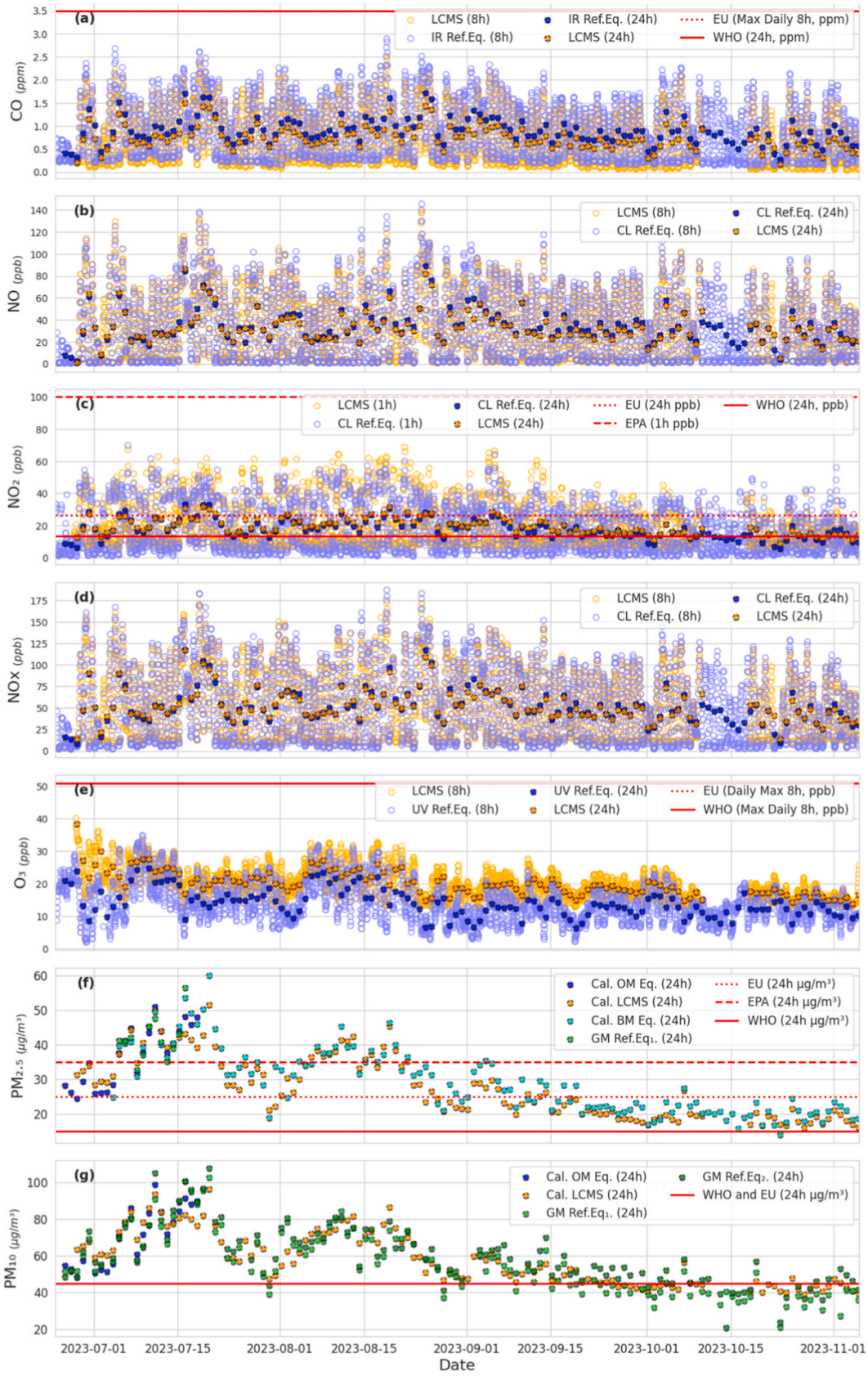

Fig. 2. Temporal variation of pollutant concentrations measured by a low-cost monitoring station (LCMS) and reference equipment (Ref.Eq.), and international air quality standards or guidelines. IR – non-dispersive infrared monitor, CL – chemiluminescence monitor, UV – non-dispersive ultraviolet monitor, Cal. OM – optical monitor (DustTrak) data corrected using gravimetric measurements, Cal. BM –Beta-attenuation monitor data corrected using gravimetric measurements, GM – gravimetric method (Eq_1. – Low-volume sampler, Eq_2. – High-volume sampler).

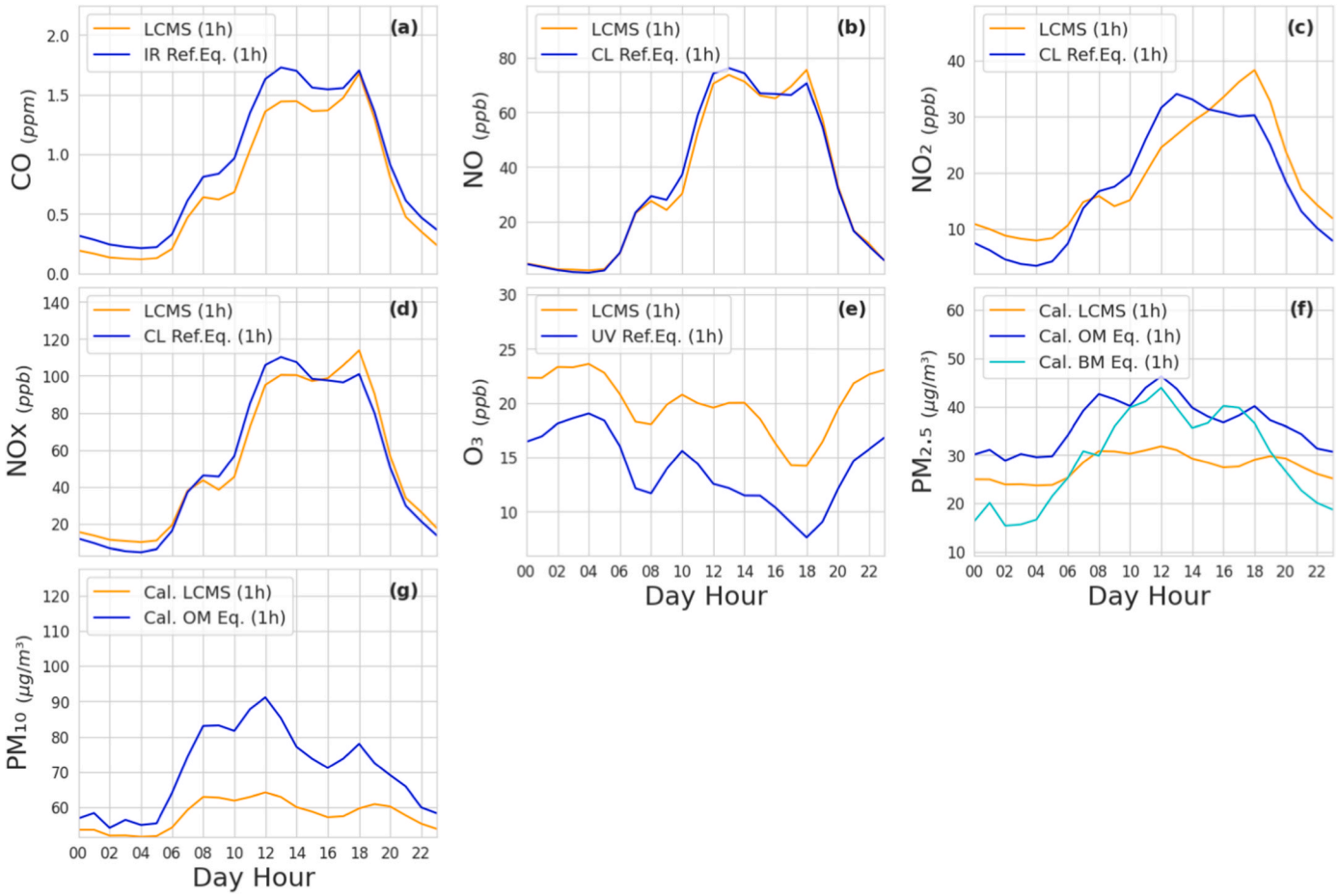

Fig. 3. Comparative daily profiles of air pollutant measurements from the low-cost monitoring station (LCMS) and reference equipment (Ref.Eq.). IR – non-dispersive infrared monitor, CL – chemiluminescence monitor, UV – non-dispersive ultraviolet monitor, Cal. OM – optical monitor (DustTrak) data corrected using gravimetric measurements, Cal. BM – Beta-attenuation monitor data corrected using gravimetric measurements.

During this campaign, CO concentrations were higher in the winter period compared to summer, as evidenced by higher values in the first three months of monitoring.

3.2.2. *Nitrogen oxides (NOx)*

NOx levels averaged 33.9 ± 40.8 ppb for NO and 17.7 ± 14.2 ppb for NO_2. Megacities typically display higher NOx emissions from vehicles and industrial activity (Liu et al., 2016; Mei et al., 2021; Nogueira et al., 2021; Xie et al., 2016). Luanda experienced NO_2 levels higher than those observed in São Paulo between 2018 and 2021, with similar daily behaviour and peaks typically occurring during traffic rush hours (Alvim et al., 2023; Moreira et al., 2023), as well as in Greater Cairo, where annual mean NO_2 concentrations ranged from approximately 20 to 63 µg m^{-3} (10–33 ppb; Hwehy et al., 2024). Comparable or even higher values have also been observed in major Indian megacities. For instance, pre-pandemic averages NO_2 concentrations in Mumbai, Delhi and Kolkata were 21.6 ± 15.1 ppb, 23.0 ± 7.6 ppb, and 26.6 ± 5.7 ppb, respectively (Mandal et al., 2021). Although no marked seasonal changes in NO_2 concentrations were registered, a significant shift was observed in September. While levels did not exceed the USEPA's hourly threshold of 100 ppb, 104 daily measurements (78% of the campaign) surpassed the WHO 24-h guideline (13.3 ppb) and 11 days (8.3%) the EU threshold (26.5 ppb), still within the 18 annual exceedances permitted by the regulation at the time of analysis.

The LCMS and chemiluminescence reference equipment (CL Ref.Eq.) showed good agreement for NOx (Fig. 4 (g): $R^2 = 0.95$ and RMSE = 12.5 ppb) and NO measurements (Fig. 4 (c): $R^2 = 0.96$, RMSE = 8.66 ppb), with a slightly lower correlation observed for NO_2 (Fig. 4 (e): $R^2 = 0.81$, RMSE = 6.35 ppb). No significant systematic bias was observed in NO measurements. However, for NO_2, the LCMS tended to underestimate hourly concentrations near 30 ppb, while showing a tendency to overestimate as values diverged from this level. Additionally, an underestimation trend was also noted in daily averages as the levels increased. An offset of about 5 ppb was observed, as the LCMS failed to record values below this limit, unlike the CL Ref.Eq. However, expecting robust correlations between the devices at low concentrations may be unrealistic due to the significant influence of noise on the signal (Zikova et al., 2017). Despite this, comparisons of NO_2 daily means between the LCMS and reference equipment were statistically consistent across NOx components.

3.2.3. *Ozone (O_3)*

Ozone concentrations averaged 14.0 ± 7.6 ppb. These values were lower than those recorded in major economic mega-regions of China, such as Beijing-Tianjin-Hebei, Yangtze River Delta, and Pearl River Delta, which include some of the largest megacities in the world. In these regions, 8-h peak ozone concentrations have historically averaged around 200 ppb, with values ranging from 70 to 286 ppb, while typical annual mean concentrations are generally between 90 and 100 ppb (Wang et al., 2017; Yang et al., 2021). In contrast, other megacities like São Paulo and suburban areas of Nanjing report lower levels (~50 ppb; Alvim et al., 2023; Xie et al., 2016). Luanda exhibited a distinct daily O_3 profile compared to typical tropospheric ozone cycles, with a diurnal peak resembling that observed in São Paulo (Alvim et al., 2023). The daily O_3 profile showed a bimodal pattern, as observed in Fig. 3 (e), with higher levels from 09:00 to 14:00 and at night. This behaviour is further

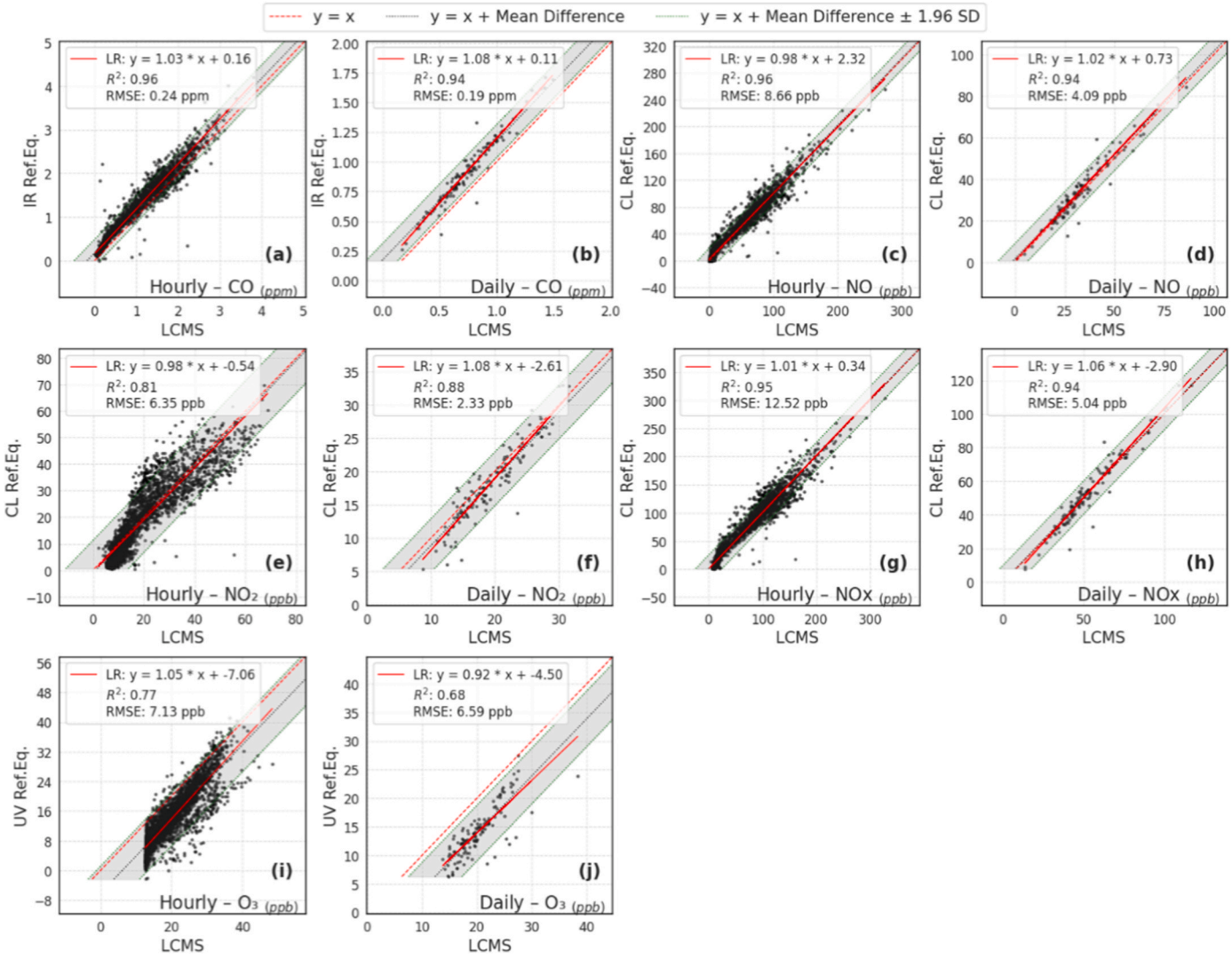

Fig. 4. Hybrid plot of linear regression (LR) and Bland–Altman analysis between measurements of the low-cost monitoring station (LCMS) and reference equipment (Ref.Eq.) for hourly and daily measurements of air pollutants. IR – non-dispersive infrared monitor, CL – chemiluminescence monitor, UV – non-dispersive ultraviolet monitor, OM – optical method (DustTrak).

evidenced by its negative correlation with SR, temperature and WS ($\rho = -0.22$, -0.31 and -0.20, respectively). Ozone, a secondary pollutant produced through photolysis involving precursors, typically shows a positive correlation with diurnal solar radiation (Yang et al., 2021; Ziemke et al., 2017). However, the data suggests that in Luanda, ozone behaviour is more strongly influenced by convective processes than SR, likely due to the transport of O_3 via a combination of vertical and horizontal mixing (Hua et al., 2021; Ziemke et al., 2017). These processes include turbulent mixing, which can bring ozone from different altitudes to the surface, by low-level jets, which occur close to the ground and can transport ozone horizontally over synoptic scale (He et al., 2023; Kulkarni et al., 2013, 2016). Measurements in Shenzhen, China, suggested that the nocturnal residual layer stores the ozone and has a remarkable impact on the surface concentrations of this pollutant on the next day (He et al., 2021). Similar behaviours have been observed in cities with high density of precursor emission sources and unique geographic features, as can be the case of Luanda (Gopi et al., 2022; He et al., 2022, 2023; Song et al., 2017; Vanesa et al., 2021). Moreover, the pattern of NO emissions throughout the day is one of the most decisive factors influencing the daily ozone profile. Under high NOx conditions, ozone production becomes highly sensitive to the interaction between NOx and O_3, where the rate of ozone destruction can increase significantly due to faster reaction rates and elevated NO levels, particularly during periods of increased temperature and photochemical activity (Coates et al., 2016; Tan et al., 2023). Seasonal trends for O_3 were similar to those of CO, showing a slight reduction in concentrations, with significant changes, from August to September. Additionally, no exceedances of the USEPA and EU limits or WHO guideline were observed.

The LCMS showed notable discrepancies in O_3 measurements compared to the non-dispersive ultraviolet reference equipment (UV Ref. Eq.), particularly at hourly concentrations below 20 ppb, likely near the method's limit of detection (LOD). As a result, a poorer agreement was expected (Fig. 4 (i): $R^2 = 0.77$, RMSE = 7.13 ppb) and a clear systematic offset was observed (Fig. 2 (e) and 3 (e)). The Bland-Altman hybrid plots revealed a pronounced proportional systematic bias that increased linearly within lower concentrations (0–15 ppb), although this trend was less pronounced for higher levels. Furthermore, the LCMS consistently overestimated concentrations compared to the reference equipment, being slightly more pronounced during daytime, coinciding with lower O_3 concentrations and higher levels of other air pollutants. This is supported by a moderate correlation between the magnitude of the discrepancy and the concentrations of other gaseous pollutants (average $\rho \approx 0.41$), while meteorological parameters exhibited a weaker association ($\rho < 0.10$). Nevertheless, both devices displayed similar

overall trends in their measurements. The offset likely stems from NO_2 cross-sensitivity (Castell et al., 2017; Croce and Tondini, 2022; Samad et al., 2020; Spinelle et al., 2015, 2017) and sensor ageing, given that the LCMS operated beyond its recommended lifespan. Samad et al. (2020) reported that while low-cost electrochemical gas sensors showed improvements in CO and NOx detection after calibration, similar adjustments for O_3 were challenging, even under steady temperature and RH conditions. Given the high concentrations of NO_2 in this campaign, cross-sensitivity effects may have been exacerbated. Therefore, in an environment with high levels of this gaseous pollutant, it would be advisable to integrate specific O_3 sensors or employ advanced calibration methods to enhance accuracy (Croce and Tondini, 2022; Spinelle et al., 2015, 2017).

3.3. Particulate matter (PM)

3.3.1. $PM_{2.5}$

Figure S6 (d) and Figure S7 (a) show that the LCMS and DustTrak (OM Eq.) presented a strong systematic bias yet maintained a consistent linear correlation for both hourly and daily measurements ($R^2 = 0.88$ and RMSE $\cong$ 75 μg m^{-3}). Factors such as relative humidity, temperature, or particle composition can systematically affect optical readings, amplifying deviations from gravimetric reference values. Optical sensors and DustTrak devices rely on light scattering, which can exaggerate mass estimates for certain particle types (e.g., sea salt, soot) relative to the true mass. When these measurements were corrected using the concentrations obtained by the gravimetric method, the RMSE decreased to 6.94 μg m^{-3}.

Although hourly concentrations from the Beta Monitor (BM Eq.) showed a low correlation with both the DustTrak and the LCMS ($R^2 \approx 0.4$), the correlation improved substantially when data were averaged to daily values ($R^2 \cong 0.87$). Inspection of the limits of agreement in Figure S7 (c) indicates that the LCMS demonstrated reasonable agreement but weak correlation with the low-volume gravimetric sampler (GM Ref. Eq_1.), showing a tendency to underestimate concentrations ($R^2 = 0.41$, RMSE = 21.6 μg m^{-3}, slope = 0.27). In comparison, the DustTrak showed a stronger correlation with the gravimetric method ($R^2 = 0.70$), despite a pronounced overestimation (RMSE 59.5 μg m^{-3}; slope = 1.71) (Figure S7 (e)). The correlation between the LCMS and the low-volume sampler (GM Ref.Eq_1.) could have been stronger if more $PM_{2.5}$ gravimetric measurements had been included in the intercomparison. This was observed when the analysis period between LCMS and the Beta monitor was extended from two weeks to four months, increasing the R^2 from 0.55 to 0.88 and the slope from 0.37 to 0.68. The correlation between BM and GM Ref.Eq. was the strongest among $PM_{2.5}$ devices ($R^2 = 0.92$ and RMSE = 9.20 μg m^{-3}). Furthermore, neither the LCMS nor the BM Eq. showed significant systematic bias, underestimating the levels when compared to the GM Ref.Eq_1.

Marine aerosols are known to influence the response of optical particle counters, as the presence of sea salt enhances the hygroscopic growth factor (HGF) of fine particles, thereby biasing optical mass estimates (Liu et al., 2023; Nurowska and Markowicz, 2023; Qiu et al., 2024; Reich et al., 2023; Zou et al., 2024). Relative humidity consistently exceeded 70% throughout the campaign. Being a coastal city, Luanda is likely influenced by marine air masses, which may enhance hygroscopic growth and lead to overestimation of particle mass by optical sensors. However, relative humidity showed no significant correlation with the measurement discrepancy between the LCMS and BM Eq. Instead, discrepancies were more strongly correlated with lower T and WS (average $\rho = -0.5$), and with higher CO and NOx levels (average $\rho = 0.66$). To minimise bias in PM measurements due to relative humidity and hygroscopic growth, DustTrak instruments can be equipped with a heated or desiccated inlet to condition the sampled air (Atfeh et al., 2025; Kang and Choi, 2024); however, such a setup was not employed in the present study. The relatively stable humidity conditions observed in this study (mean ≈ 80%, daily STD ≈ 3%) may have produced a nearly constant bias, which was largely accounted for the linear calibration (Crilley et al., 2019; Magi et al., 2020). This highlights the complexity of humidity effects on optical particle sensors: while heated inlets can eliminate much of the HGFs, under conditions of stable high humidity a simple linear correction may also be sufficient. Even so, relying solely on RH for calibration can lead to inadequate corrections and compromise accuracy, underscoring the need for calibration strategies that integrate multiple environmental factors (Brattich et al., 2020; Hua et al., 2021; Lopes et al., 2020; Zafra-Pérez et al., 2022). In this study, it was observed that lower temperature ($\rho = -0.8$) and WS ($\rho = -0.6$) were associated with higher $PM_{2.5}$ levels. This can be explained because both factors, when increased, tend to promote stronger air turbulence, which facilitates the dispersion of $PM_{2.5}$ and, consequently, the decrease of its concentration. Additionally, higher temperatures stimulate the evaporation of some $PM_{2.5}$ components, such as water vapour, nitrate, and ammonium, which contributes to a decrease in $PM_{2.5}$ levels. Higher temperatures also lead to increased emissions of biogenic non-methane volatile organic compounds (NMVOCs). As NMVOC levels rise, more hydroxyl radicals are consumed in the formation of biogenic secondary organic aerosols, limiting the oxidation of SO_2 and the formation of sulphate in $PM_{2.5}$ (Nguyen et al., 2024). The measurement discrepancy between the LCMS and BM Eq. was more strongly correlated with lower T and WS (average $\rho = -0.5$), and with higher CO and NOx levels (average $\rho = 0.66$).

Given that the best agreement was obtained between the beta monitor and the gravimetric samplers, the correlation between them was used to correct the data of beta-monitor and then interpret the temporal variations in $PM_{2.5}$ concentrations. The average $PM_{2.5}$ concentration was 29.0 ± 9.4 μg m^{-3}. The highest average daily concentration was registered in July (59.8 μg m^{-3}), whereas the lowest (13.9 μg m^{-3}) was observed in October, which was the only day that did not exceed the 24-h WHO guideline of 15 μg m^{-3}. This guideline was surpassed in 99.2% of the monitoring days. The EU daily limit (25 μg m^{-3}) and the 24-h USEPA standard (35 μg m^{-3}) were exceeded on 66 and 32 out of the 125 days, respectively. The USEPA standard for the 98th percentile of 1-h daily maximum concentrations, averaged over 3 years, was not observed either. The average $PM_{2.5}$ concentration recorded during the monitoring campaign is in line with values reported for other megacities, including São Paulo, Osaka, Kinshasa, Hong Kong, and Chinese megaregions, ranging from 23.7 to 51.3 μg m^{-3} (Alvim et al., 2023; Jahn et al., 2011; McFarlane et al., 2021; Moreira et al., 2023; Nakata et al., 2015; Yang et al., 2021). However, it remained lower than the levels reported for Lagos, Delhi, Zhengzhou and Guangzhou (>80 μg m^{-3}; Gahungu et al., 2022; Guttikunda et al., 2023; Jahn et al., 2011). The high levels of $PM_{2.5}$ recorded during the "cacimbo" season should be a cause for great concern and alert, pointing to the urgent need to take measures to protect the health of the population.

3.3.2. PM_{10}

PM_{10} levels of 58.4 ± 16.5 μg m^{-3} were recorded. On some days, concentrations greater than 100 μg m^{-3} were observed, specifically from July to August, with September marking a significant change. The lowest daily concentration of 20.9 μg m^{-3} was recorded in October. On average, PM_{10} concentrations were twice as high as some annual averages recorded in São Paulo, but very similar to those reported for Hong Kong, Seoul, Johannesburg and urban background of Beijing (Alvim et al., 2023; Choi and Choi, 2022; Gao et al., 2019; Moreira et al., 2023). However, many cities have recorded annual averages above 100 μg m^{-3}, such as Beijing, Delhi, Chengdu and Guangzhou (Feng et al., 2021; Jahn et al., 2011; Liu et al., 2019). Additionally, non-megacities like Faisalabad, Kashi, and Hetian have documented annual averages greater than 250 μg m^{-3} (Aslam et al., 2020; Liu et al., 2019). The weekly profile showed that the highest concentrations were recorded on Tuesday, while the lowest values were observed on Sunday, although the difference was not statistically significant, in line with previous studies in other regions (Campos et al., 2021). A positive correlation between PM

and NOx and CO concentrations (average $\rho = 0.5$) suggests a significant anthropogenic contribution, most likely related to road traffic. Correlations between devices varied depending on the measurement principle. The low-volume sampler (GM Ref.Eq_1.) and the high-volume sampler (GM Ref. Eq_2.) correlated well ($R^2 = 0.93$ and RMSE = 6.1 μg m^{-3}) without systematic bias (Figure S8 (f)), underscoring their reliability as reference methods, despite differences in sampling flows and filter types. However, two outliers were identified that fell significantly outside the Bland-Altman limits of agreement, with no clear explanation for their deviation. They may have been caused by random errors during the weighing process. In contrast, the comparison between the LCMS and DustTrak revealed a significant systematic bias, with discrepancies increasing at higher concentration levels. However, the LCMS showed a strong linear correlation with the DustTrak (OM Eq_1) ($R^2 = 0.83$ hourly; $R^2 = 0.94$ daily).

The LCMS (Figure S8 (b) and (c)) showed greater bias than the DustTrak (OM Eq_1.) (Figure S8 (d) and (e)) against GM. However, their responses differed: the OM Eq. (DustTrak) tended to overestimate PM_{10} concentrations (average slope = 1.28), whereas the LCMS consistently underestimated them (average slope = 1.28). Additionally, OM Eq. demonstrated a closer alignment with GM, especially with the low-volume sampler (GM Ref.Eq_1.). The daily gravimetric measurements yielded a high coefficient of determination for the relationship with the DustTrak ($R^2 = 0.91$) and, to a lesser extent, with the LCMS ($R^2 = 0.76$).

Based on the gravimetric samplers, Luanda exceeded the EU daily limit and the WHO guideline for PM_{10} on 91 days out of 121. Daily concentrations from the low-cost sensor did not exceed legislated or recommended values, highlighting the challenge optical monitors face in accurately capturing concentration magnitudes without gravimetric correction, since the RMSE could be significant. This discrepancy suggests potential underestimation by the LCMS or overestimation by the DustTrak, which may misrepresent health risks. However, the LCMS has demonstrated its long-term stability, making it adequate under high pollutant concentrations and suitable for identifying PM "hot spots" (Badura et al., 2018; Castell et al., 2017; Han et al., 2021).

3.4. Evaluation of linear and non-linear calibration approaches

Daily averages consistently produced better agreement than hourly data, as evidenced by narrower Bland–Altman intervals and markedly lower RMSE values. For example, the RMSE for CO decreased from 0.24 ppm (hourly) to 0.19 ppm (daily), while NOx exhibited an even larger relative improvement (12.5 ppb–5.04 ppb). Similarly, O_3 RMSE decreased from 7.13 ppb at hourly resolution to 6.59 ppb for daily data. These reductions in error were not always mirrored by R^2 values, which sometimes declined slightly (e.g., NO_2: 0.87 hourly vs. 0.88 daily). This highlights that averaging improves absolute accuracy by reducing random noise, although it does not necessarily increase correlation strengths (Huang, 2023).

Table 1 presents the main statistical parameters used in the analysis, such as R^2 and RMSE, while Table S2 (in the supplementary material) provides the corresponding calibration equations. When evaluating calibration methods for gas measurements, ordinary linear regression (OLR) produced substantial improvements over raw LCMS data, particularly for NO and NOx, for which OLR offered greater interpretability. For CO, the RMSE decreased from 0.19 ppm (raw daily) to 0.07 ppm after OLR calibration, while for O_3, the RMSE was reduced from 7.13 to 3.68 ppb (hourly). Multiple linear regression (MLR) generally provided only marginal improvements beyond those achieved with OLR. The most significant gains, however, were observed for hourly NO_2 and O_3 concentrations when using artificial neural networks (NN). For NO_2 (hourly), OLR and MLR performed similarly ($R^2 = 0.81$; RMSE = 6.26 ppb), but the NN further increased R^2 to 0.87, reduced RMSE to 5.1 ppb, and, importantly, corrected the inflection in the regression pattern observed in Bland–Altman residual analyses at (~30 ppm). For hourly O_3 measurements, both MLR and NN enhanced the estimation of low concentrations near the limit of detection (below 20 ppb), with the NN achieving the best overall performance (RMSE = 3.1 ppb; $R^2 = 0.83$). These findings indicate that cross-sensitivities among gases are especially relevant for O_3, which depends strongly on NOx chemistry, whereas meteorological parameters such as RH and SR primarily modulate the response of CO. OLRs generally sufficed to improve accuracy across pollutants, with minimal additional benefit from MLRs, except for O_3 (Fig. S9). For O_3, both OLR and MLR reduced the RMSE from 7.13 (raw) to 3.4 ± 0.13 (fitted). Although MLR produced results similar to OLR, it was the only pollutant for which MLR offered further improvement, particularly when incorporating NOx-related variables into the calibration model. This approach improved recovery of values below 20 ppb and highlighted the importance of accounting for O_3 and NO_2 cross-sensitivity.

Table 1
Performance of LCMS against reference instruments (gas analysers, DustTrak, Beta Monitor, Low-volume sampler (LVS) and High-volume sampler (HVS) by gravimetric methods (GM) expressed as RMSE and R^2 before and after calibration using ordinary linear regression (OLR), multi-linear regression (MLR) with LCMS data or reference-based, and artificial neural network (NN) models at daily and hourly resolutions.

	LCMS vs Ref	*RMSE (Raw)*	*R^2 and RMSE (OLR)*		*R^2 and RMSE (MLR-LCMS)*		*R^2 and RMSE (MLR-Ref.)*		*R^2 and RMSE (NN-Ref)*	
Daily	RH	2.4%	0.87	1.1%	0.93	0.80%	0.95	0.67%	0.95	0.67%
	Temp	1.4 °C	0.98	0.21 °C	0.98	0.21 °C	0.98	0.21 °C	0.98	0.21 °C
	CO	0.19 ppm	0.94	0.07 ppm	0.94	0.07 ppm	0.96	0.05 ppm	0.95	0.06 ppm
	NO	4.1 ppb	0.94	3.8 ppb	0.94	3.8 ppb	0.94	3.8 ppb	0.91	4.5 ppb
	NO_2	2.3 ppb	0.88	2.0 ppb	0.88	2.0 ppb	0.88	2.0 ppb	0.85	2.2 ppb
	NOx	5.0 ppb	0.94	4.9 ppb	0.94	4.9 ppb	0.94	4.9 ppb	0.91	6.1 ppb
	O_3	6.6 ppb	0.68	2.5 ppb	0.71	2.4 ppb	0.71	2.3 ppb	0.76	2.1 ppb
	DustTrak ($PM_{2.5}$)	74.4 μg m^{-3}	0.88	6.9 μg m^{-3}	0.95	4.5 μg m^{-3}	0.97	3.2 μg m^{-3}	0.96	4.2 μg m^{-3}
	Beta Monitor ($PM_{2.5}$)	11.2 μg m^{-3}	0.89	2.8 μg m^{-3}	0.92	2.3 μg m^{-3}	0.92	2.3 μg m^{-3}	0.96	1.75 μg m^{-3}
	Low volume sampler ($PM_{2.5}$)	21.6 μg m^{-3}	0.41	4.6 μg m^{-3}	0.88	2.0 μg m^{-3}	0.88	2.2 μg m^{-3}	0.43	4.5 μg m^{-3}
	DustTrak (PM_{10})	82.9 μg m^{-3}	0.89	7.1 μg m^{-3}	0.95	4.7 μg m^{-3}	0.96	4.4 μg m^{-3}	0.92	6.0 μg m^{-3}
	Low volume sampler (PM_{10})	46.4 μg m^{-3}	0.82	7.3 μg m^{-3}	0.88	6.0 μg m^{-3}	0.86	6.5 μg m^{-3}	0.88	6.1 μg m^{-3}
	High volume sampler (PM_{10})	50.4 μg m^{-3}	0.76	7.6 μg m^{-3}	0.84	6.3 μg m^{-3}	0.82	6.6 μg m^{-3}	0.66	9.1 μg m^{-3}
Hourly	RH	3.1%	0.92	2.3%	0.96	1.6%	0.97	1.5%	0.98	1.2%
	Temp	1.48 °C	0.94	0.60 °C	0.96	0.48 °C	0.96	0.49 °C	0.96	0.45 °C
	CO	0.24 ppm	0.96	0.16 ppm	0.97	0.14 ppm	0.97	0.14 ppm	0.97	0.13 ppm
	NO	8.7 ppb	0.96	8.5 ppb	0.96	8.4 ppb	0.96	8.0 ppb	0.97	7.3 ppb
	NO_2	6.4 ppb	0.81	6.3 ppb	0.81	6.3 ppb	0.81	6.3 ppb	0.87	5.1 ppb
	NOx	12.5 ppb	0.95	12.5 ppb	0.95	12.5 ppb	0.95	12.5 ppb	0.96	11.1 ppb
	O_3	7.1 ppb	0.77	3.7 ppb	0.8	3.4 ppb	0.81	3.4 ppb	0.83	3.1 ppb
	DustTrak ($PM_{2.5}$)	76.4 μg m^{-3}	0.87	10.8 μg m^{-3}	0.96	6.1 μg m^{-3}	0.97	5.5 μg m^{-3}	0.98	4.63 μg m^{-3}
	Beta Monitor ($PM_{2.5}$)	16.8 μg m^{-3}	0.39	12.5 μg m^{-3}	0.5	11.3 μg m^{-3}	0.53	11 μg m^{-3}	0.57	10.6 μg m^{-3}

For PM, OLR alone effectively addressed the primary limitation of LCMS measurements, specifically, correcting the flat density assumption used to convert particle number concentrations to mass (Castell et al., 2017; Jiang et al., 2021; Njalsson and Novosselov, 2018). Strong correlations were obtained when compared with DustTrak, reaching $R^2 = 0.97$ for $PM_{2.5}$, although this reflects consistency between methods sharing the same principle. When evaluated against GM Ref. Eq. (LVS and HVS), performance was more modest: for $PM_{2.5}$, MLR-calibration improved R^2 from 0.41 to 0.88 (LVS), with RMSE reduced to ~2 μg m^{-3}, while for PM_{10} the best results reached $R^2 \approx 0.84–0.88$ and RMSE ≈ 6 μg m^{-3}. Examination of the regression models revealed that calibration systematically incorporated meteorological and gaseous parameters, indicating that residual errors are strongly modulated by environmental interactions: at the daily scale, predictors such as T, WS and CO were consistently retained, highlighting the combined effects of hygroscopic growth and combustion tracers on bias formation (Sá et al., 2022; Wang et al., 2024), whereas at the hourly scale $PM_{2.5}$ variability was more closely tied to short-term interactions with CO, O_3 and NO_2 together with solar radiation (SR) (Fig. S9). Although non-linear approaches (e.g., humidity compensation and pollutant cross-sensitivities) can provide robust improvements (Zheng et al., 2018), in our dataset, relative humidity and gaseous covariates may have exhibited strong multicollinearity with another variable, suggesting that their effects were already incorporated within the regression structure, such as, in the O_3 equations. Furthermore, with very limited sample sizes ($n < 20$), the NN-MLP systematically underperformed, consistent with the known instability of neural networks under data-sparse conditions.

While OLR and MLR provide practical calibration approaches for most pollutants - particularly CO and PM - advanced machine learning techniques offer greater robustness, especially for NO_2 and O_3, which are more prone to cross-sensitivities. Machine learning, and artificial neural networks in particular, offer more promising and robust calibration strategies; however, this comes at the cost of reduced interpretability and the need for careful selection of calibration periods (Chojer et al., 2020; Han et al., 2021; Liang, 2021). Liang (2021) observed that there is no universal calibration method for low-cost sensors, as their performance is highly dependent on pollutant type, environmental conditions, and calibration duration. Moreover, the researcher emphasised the lack of calibration studies in highly polluted but underserved regions, which limits model generalisability and underlines the need for more geographically diverse and context-specific calibration protocols.

4. Conclusions

This study provides one of the first continuous, ground-level assessments of meteorological and atmospheric pollutants (CO, O_3, NOx, PM_{10}, $PM_{2.5}$, and PM_1) in Luanda, Angola, a rapidly urbanising city that currently lacking formal air quality monitoring infrastructure. The data revealed critical peaks in pollutant concentrations, with frequent exceedances of WHO and EU recommended limits for PM_{10}, $PM_{2.5}$, and NO_2. These findings indicate serious public health risks and the urgent need for mitigation strategies and stricter regulatory measures.

The performance assessment of the low-cost monitoring station (LCMS) against reference equipment yielded mixed results. Strong agreements were observed for CO and meteorological parameter measurements, while NOx measurements showed good agreement overall, though with limitations near detection limits. However, significant challenges were identified, particularly for O_3, whose measurements were compromised by strong cross-sensitivity with NO_2, further exacerbated by the high concentrations of the latter in Luanda, and potential sensor ageing. For particulate matter (PM_{10} and $PM_{2.5}$), despite the good R^2 obtained between the LCMS and reference methods (gravimetric and beta-attenuation), considerable systematic deviations and high RMSE were observed. These biases can be effectively addressed using multiple linear regression (MLR), which provides interpretable results and robust statistical performance compared with neural networks. The pollutants that benefitted most from neural network calibration were NO_2 and O_3. These findings reinforce the critical need for continuous calibration, rigorous validation, and the application of correction models (such as MLR and NN) to LCMS data, particularly for O_3 and PM, to ensure their reliability for long-term monitoring.

Despite inherent limitations, primarily related to quantitative accuracy for O_3 and PM in the absence of pollutant-specific calibration, the LCMS proved to be a promising and cost-effective tool for expanding air quality monitoring. Its practical application, however, depends on careful data processing and calibration to overcome biases from cross-sensitivities and environmental factors. Its ability to provide real-time data and long-term stability, as observed for NOx, CO and PM, supports its viable as a complementary alternative to reference-grade monitoring networks. The LCMS is particularly valuable for increasing the spatial density of monitoring, identifying pollution 'hotspots', and supporting air quality management, especially in resource-limited regions, if its uncertainties are properly characterised and mitigated through appropriate calibration and validation procedures.

CRediT authorship contribution statement

Alan Victor da Silva: Writing – original draft, Investigation, Formal analysis, Data curation. **Leonardo Furst:** Investigation, Data curation. **Yago A. Cipoli:** Investigation. **Marlene J.S. Soares:** Investigation. **Anabela G.A. Leitão:** Writing – review & editing, Resources. **Manuel Feliciano:** Writing – review & editing, Supervision, Resources, Methodology, Funding acquisition, Conceptualization. **Célia A. Alves:** Writing – review & editing, Supervision, Resources, Project administration, Methodology, Funding acquisition, Conceptualization.

Data availability

Data will be made available on request

Declaration of competing interest

The authors declare the following financial interests/personal relationships which may be considered as potential competing interests: Alan Victor da Silva reports financial support and article publishing charges were provided by Foundation for Science and Technology. If there are other authors, they declare that they have no known competing financial interests or personal relationships that could have appeared to influence the work reported in this paper.

Acknowledgments

This work was supported by the Portuguese Foundation for Science and Technology (FCT) through the PhD fellowships 2023.02059.BD, 2023.04826.BD, SFRH/BD/04992/2021 and SRFH/BD/08461/2020. The research was performed in the frame of the project APAM, financially supported by national funds (OE), through FCT/MCTES (DOI: 10.54499/2022.04240.PTDC). This work was also financed by national funds through FCT under the project/grant UID/50006 + LA/P/0094/2020 (doi.org/10.54499/LA/P/0094/2020), and through FCT/MCTES (PIDDAC): CIMO, UIDB/00690/2020 (DOI: 10.54499/UIDB/00690/2020); and SusTEC, LA/P/0007/2020 (DOI: 10.54499/LA/P/0007/2020). We would also like to sincerely thank d·nota® and bettair® for providing the equipment used in our tests. Additionally, we would like to thank the Faculty of Engineering of the Agostinho Neto University for providing the logistical conditions for carrying out the monitoring campaign in Luanda.

Appendix A. Supplementary data

Supplementary data to this article can be found online at https://doi.

org/10.1016/j.apr.2025.102746.

References

Aggoune-Mtalaa, W., Laib, M., 2023. Analyzing air pollution and traffic data in urban areas in Luxembourg. Smart Cities 6, 929–943. https://doi.org/10.3390/smartcities6020045.

Alvarez, C.M., Hourcade, R., Lefebvre, B., Pilot, E., 2020. A scoping review on air quality monitoring, policy and health in West African cities. Int. J. Environ. Res. Publ. Health 17, 1–28. https://doi.org/10.3390/ijerph17239151.

Alvim, D.S., Herdies, D.L., Corrêa, S.M., Basso, L.S., Khalid, B., Silva, G.F.P., Oyerinde, G., de Carvalho, N.A., Coelho, S.M. S. da C., Figueroa, S.N., 2023. COVID-19 pandemic: impacts on air quality during partial lockdown in the metropolitan area of São Paulo. Remote Sens. 15, 1262. https://doi.org/10.3390/rs15051262.

Amegah, A.K., Dakuu, G., Jaakkola, J.J.K., 2018. Proliferation of low-cost sensors: what prospects for air quality monitoring in Sub-Saharan Africa? Environ. Res. 167, 475–484. https://doi.org/10.1016/j.envres.2018.08.008.

Aslam, A., Ibrahim, M., Shahid, I., Mahmood, A., Irshad, M.K., Yamin, M., Ghazala, Tariq, M., Shamshiri, R.R., 2020. Pollution characteristics of particulate matter ($PM_{2.5}$ and PM_{10}) and constituent carbonaceous aerosols in a South Asian future megacity. Appl. Sci. 10, 1–17. https://doi.org/10.3390/app10248864.

Atfeh, B., Barcza, Z., Groma, V., Tordai, Á.V., Mészáros, R., 2025. Performance assessment of low- and medium-cost PM2.5 sensors in real-world conditions in Central Europe. Atmosphere 16, 796. https://doi.org/10.3390/atmos16070796.

Atuhaire, C., Gidudu, A., Bainomugisha, E., Mazimwe, A., 2022. Determination of satellite-derived $PM_{2.5}$ for Kampala District, Uganda. Geomatics 2, 125–143. https://doi.org/10.3390/geomatics2010008.

Atuyambe, L., Okello, G., Sematimba, D., Ssematimba, A., 2024. Technological advancement and the emergence of low-cost sensors promise to improve air quality data availability in the region. Ann. Glob. Health 90 (1), 10. https://doi.org/10.5334/aogh.4527.

Badura, M., Batog, P., Drzeniecka-Osiadacz, A., Modzel, P., 2018. Optical particulate matter sensors in $PM_{2.5}$ measurements in atmospheric air. In: E3S Web of Conf. EDP Sciences, 00006. https://doi.org/10.1051/e3sconf/20184400006.

Bai, K., Li, K., Chang, N. Bin, Gao, W., 2019. Advancing the prediction accuracy of satellite-based $PM_{2.5}$ concentration mapping: a perspective of data mining through in situ $PM_{2.5}$ measurements. Environ. Pollut. 254, 113047. https://doi.org/10.1016/j.envpol.2019.113047.

Bauer, S.E., Im, U., Mezuman, K., Gao, C.Y., 2019. Desert dust, industrialization, and agricultural fires: health impacts of outdoor air pollution in Africa. J. Geophys. Res. Atmos. 124, 4104–4120. https://doi.org/10.1029/2018JD029336.

Bikkina, S., Andersson, A., Kirillova, E.N., Holmstrand, H., Tiwari, S., Srivastava, A.K., Bisht, D.S., Gustafsson, Ö., 2019. Air quality in megacity Delhi affected by countryside biomass burning. Nat. Sustain. 2, 200–205. https://doi.org/10.1038/s41893-019-0219-0.

Brattich, E., Bracci, A., Zappi, A., Morozzi, P., Sabatino, S. Di, Porcù, F., Nicola, F. Di, Tositti, L., 2020. How to get the best from low-cost particulate matter sensors: guidelines and practical recommendations. Sensors 20, 1–33. https://doi.org/10.3390/s20113073.

Campos, P.M.D., Esteves, A.F., Leitão, A.A., Pires, J.C.M., 2021. Design of air quality monitoring network of Luanda, Angola: urban air pollution assessment. Atmos. Pollut. Res. 12, 101128. https://doi.org/10.1016/j.apr.2021.101128.

Cassiani, M., Stohl, A., Eckhardt, S., 2013. The dispersion characteristics of air pollution from the world's megacities. Atmos. Chem. Phys. 13, 9975–9996. https://doi.org/10.5194/acp-13-9975-2013.

Castell, N., Dauge, F.R., Schneider, P., Vogt, M., Lerner, U., Fishbain, B., Broday, D., Bartonova, A., 2017. Can commercial low-cost sensor platforms contribute to air quality monitoring and exposure estimates? Environ. Int. 99, 293–302. https://doi.org/10.1016/j.envint.2016.12.007.

Choi, S.M., Choi, H., 2022. Artificial neural network modeling on PM_{10}, $PM_{2.5}$, and NO_2 concentrations between two megacities without a lockdown in Korea, for the COVID-19 pandemic period of 2020. Int. J. Environ. Res. Publ. Health 19, 16338. https://doi.org/10.3390/ijerph192316338.

Chojer, H., Branco, P.T.B.S., Martins, F.G., Alvim-Ferraz, M.C.M., Sousa, S.I.V., 2020. Development of low-cost indoor air quality monitoring devices: recent advancements. Sci. Total Environ. 727, 138385. https://doi.org/10.1016/j.scitotenv.2020.138385.

Clements, A.L., Reece, S., Conner, T., Williams, R., 2019. Observed data quality concerns involving low-cost air sensors. Atmos. Environ. X 3, 100034. https://doi.org/10.1016/j.aeaoa.2019.100034.

Coates, J., Mar, K.A., Ojha, N., Butler, T.M., 2016. The influence of temperature on ozone production under varying NOx conditions - a modelling study. Atmos. Chem. Phys. 16, 11601–11615. https://doi.org/10.5194/acp-16-11601-2016.

Crilley, L., Singh, A., Kramer, L., Shaw, M., Alam, M., Apte, J., Bloss, W., Ruiz, L., Fu, P., Fu, W., Gani, S., Gatari, M., Ilyinskaya, E., Lewis, A., Ng'ang'a, D., Sun, Y., Whitty, R., Yue, S., Young, S., Pope, F., 2019. Effect of aerosol composition on the performance of low-cost optical particle counter correction factors. Atmos. Meas. Tech. 13, 1181–1193. https://doi.org/10.5194/amt-13-1181-2020.

Croce, S., Tondini, S., 2022. Fixed and mobile low-cost sensing approaches for microclimate monitoring in urban areas: a preliminary study in the city of Bolzano (Italy). Smart Cities 5, 54–70. https://doi.org/10.3390/smartcities5010004.

Cushing, L., Morello-Frosch, R., Wander, M., Pastor, M., 2015. The haves, the have-nots, and the health of everyone: the relationship between social inequality and environmental quality. Annu. Rev. Publ. Health 36, 193–209. https://doi.org/10.1146/annurev-publhealth-031914-122646.

deSouza, P., Kahn, R., Stockman, T., Obermann, W., Crawford, B., Wang, A., Crooks, J., Li, J., Kinney, P., 2022. Calibrating networks of low-cost air quality sensors. Atmos. Meas. Tech. 15, 6309–6334. https://doi.org/10.5194/amt-15-6309-2022.

di Meane, E.A., Plassa, M., Rolle, F., Sega, M., 2009. Metrological traceability in gas analysis at I.N.Ri.M: gravimetric primary gas mixtures. Accred Qual. Assur. 14, 607–611. https://doi.org/10.1007/s00769-009-0577-9.

Díaz-Álvarez, E.A., de la Barrera, E., 2020. Isotopic biomonitoring of anthropic carbon emissions in a megalopolis. PeerJ 8, 9283. https://doi.org/10.7717/peerj.9283.

European Commission (EC), 2011. Commission implementing decision of 12 December 2011 laying down rules for directives 2004/107/EC and 2008/50/EC of the European Parliament and of the council as regards the reciprocal exchange of information and reporting on ambient air quality. Off. J. Eur. Union L 335/86. Luxenbourg.

European Committee for Standardizantion (CEN), 2023. EN 12341:2023 Ambient air - Standard gravimetric measurement method for the determination of the PM_{10} or $PM_{2.5}$ mass concentration of suspended particulate matter. Brussels.

European Parliament and Council of the European Union, 2024. Directive (EU) 2024/2881 of the European Parliament and of the Council of 23 October 2024 on ambient air quality and cleaner air for Europe (recast). Off. J. Eur. Union L 2881, 2881. Luxenbourg.

Feng, X., Tian, Y., Xue, Q., Song, D., Huang, F., Feng, Y., 2021. Measurement report: spatiotemporal and policy-related variations of $PM_{2.5}$ composition and sources during 2015-2019 at multiple sites in a Chinese megacity. Atmos. Chem. Phys. 21, 16219–16235. https://doi.org/10.5194/acp-21-16219-2021.

Fisher, S., Bellinger, D.C., Cropper, M.L., Kumar, P., Binagwaho, A., Biao Koudenoukpo, J., Park, Y., Taghian, G., Landrigan, P.J., 2021. Air pollution and development in Africa: impacts on health, the economy and human capital. Lancet Planet. Health 5, e681–e688. https://doi.org/10.1016/s2542-5196(21)00201-1.

Fuller, R., Landrigan, P.J., Balakrishnan, K., Bathan, G., Bose-O'Reilly, S., Brauer, M., Caravanos, J., Chiles, T., Cohen, A., Corra, L., Cropper, M., Ferraro, G., Hanna, J., Hanrahan, D., Hu, H., Hunter, D., Janata, G., Kupka, R., Lanphear, B., Lichtveld, M., Martin, K., Mustapha, A., Sanchez-Triana, E., Sandilya, K., Schaefli, L., Shaw, J., Seddon, J., Suk, W., Téllez-Rojo, M.M., Yan, C., 2022. Pollution and health: a progress update. Lancet Planet. Health 6, e535–e547. https://doi.org/10.1016/S2542-5196(22)00090-0.

Gahungu, P., Kubwimana, J.R., Muhimpundu, L.J.M.B., Ndamuzi, E., 2022. Modelling spatio-temporal trends of air pollution in Africa. arXiv:2208.12719. https://doi.org/10.48550/arXiv.2208.12719.

Gao, S., Cong, Z., Yu, H., Sun, Y., Mao, J., Zhang, H., Ma, Z., Azzi, M., Yang, W., Jiang, Y., Chen, L., Bai, Z., 2019. Estimation of background concentration of PM in Beijing using a statistical integrated approach. Atmos. Pollut. Res. 10, 858–867. https://doi.org/10.1016/j.apr.2018.12.014.

Giordano, M.R., Malings, C., Pandis, S.N., Presto, A.A., McNeill, V.F., Westervelt, D.M., Beekmann, M., Subramanian, R., 2021. From low-cost sensors to high-quality data: a summary of challenges and best practices for effectively calibrating low-cost particulate matter mass sensors. J. Aerosol Sci. 158, 105833. https://doi.org/10.1016/j.jaerosci.2021.105833.

Gopi, D., Pranesha, T.S.R., Chate, D.M., Beig, G., 2022. Analysis of ozone photochemistry over southern tropical megacity, Bengaluru, India. Photochem. Photobiol. 98, 1312–1322. https://doi.org/10.1111/php.13626.

Gualtieri, G., Ahbil, A., Rossi, A., Crisci, A., Di Sabatino, S., Toscano, P., 2024. Potential of low-cost PM monitoring sensors to fill monitoring gaps in areas of Sub-Saharan Africa. Atmos. Pollut. Res. 15 (3), 101882. https://doi.org/10.1016/j.apr.2024.101882.

Guttikunda, S.K., Dammalapati, S.K., Pradhan, G., Krishna, B., Jethva, H.T., Jawahar, P., 2023. What is polluting Delhi's air? A review from 1990 to 2022. Sustainability 15, 4209. https://doi.org/10.3390/su15054209.

Han, P., Mei, H., Liu, D., Zeng, N., Tang, X., Wang, Y., Pan, Y., 2021. Calibrations of low-cost air pollution monitoring sensors for CO, NO_2, O_3, and SO_2. Sensors 21, 1–18. https://doi.org/10.3390/s21010256.

He, C., Lu, X., Wang, Haolin, Wang, Haichao, Li, Y., He, G., He, Y., Wang, Y., Zhang, Y., Liu, Y., Fan, Q., Fan, S., 2022. The unexpected high frequency of nocturnal surface ozone enhancement events over China: characteristics and mechanisms. Atmos. Chem. Phys. 22, 15243–15261. https://doi.org/10.5194/acp-22-15243-2022.

He, G., Deng, T., Wu, D., Wu, C., Huang, X., Li, Z., Yin, C., Zou, Y., Song, L., Ouyang, S., Tao, L., Zhang, X., 2021. Characteristics of boundary layer ozone and its effect on surface ozone concentration in Shenzhen, China: a case study. Sci. Total Environ. 791, 148044. https://doi.org/10.1016/j.scitotenv.2021.148044.

He, G., He, C., Wang, Haofan, Lu, X., Pei, C., Qiu, X., Liu, C., Wang, Y., Liu, N., Zhang, J., Lei, L., Liu, Y., Wang, Haichao, Deng, T., Fan, Q., Fan, S., 2023. Nighttime ozone in the lower boundary layer: insights from 3-year tower-based measurements in South China and regional air quality modeling. Atmos. Chem. Phys. 23, 13107–13124. https://doi.org/10.5194/acp-23-13107-2023.

Health Effects Institute, 2024. State of Global Air 2024: Special Report. Boston, USA.

Hua, J., Zhang, Yuanxun, de Foy, B., Mei, X., Shang, J., Zhang, Yang, Sulaymon, I.D., Zhou, D., 2021. Improved $PM_{2.5}$ concentration estimates from low-cost sensors using calibration models categorized by relative humidity. Aerosol Sci. Technol. 55, 600–613. https://doi.org/10.1080/02786826.2021.1873911.

Huang, G., 2023. Missing data imputation strategies: a comparative analysis of hourly and daily pollution models. Atmos. Environ., 120121 https://doi.org/10.1016/j.atmosenv.2023.120121.

Hwehy, M.M.A., Moursy, F.I., El-Tantawi, A.M., Mohamed, M.A.E.-H., 2024. Evaluation of the air quality in arid climate megacities (case study: greater Cairo). Contrib. Geophys. Geodes. 54, 95–118. https://doi.org/10.31577/congeo.2024.54.1.6.

IQAir, 2020. 2020 world air quality report region & city $PM_{2.5}$ ranking. https://www.iqair.com/dl/pdf-reports/world-air-quality-report-2020-en.pdf?srsltid=AfmBOopEErFolxNwSvMnLkftQI_7treXuVFcLM65cMcSgj0D3XJVgrb5. May 2025.
Jahn, H.J., Schneider, A., Breitner, S., Eißner, R., Wendisch, M., Krämer, A., 2011. Particulate matter pollution in the megacities of the Pearl River Delta, China - a systematic literature review and health risk assessment. Int. J. Hyg Environ. Health 214, 281–295. https://doi.org/10.1016/j.ijheh.2011.05.008.
Jiang, Y., Zhu, X., Chen, C., Ge, Y., Wang, W., Zhao, Z., Cai, J., Kan, H., 2021. On-field test and data calibration of a low-cost sensor for fine particles exposure assessment. Ecotoxicol. Environ. Saf. 211, 111958. https://doi.org/10.1016/j.ecoenv.2021.111958.
Kang, J., Choi, K., 2024. Calibration methods for low-cost particulate matter sensors considering seasonal variability. Sensors 24, 3023. https://doi.org/10.3390/s24103023.
Kebede, A.A., Friberg, J., Isaxon, C., Jerrett, M., Abera, A., Malmqvist, E., Sjöström, C., Taj, T., Vargas, A.M., 2021. Air quality in Africa: public health implications article in annual review of public health. Annu. Rev. Publ. Health 42, 193–210. https://doi.org/10.1146/annurev-publhealth100119-113802.
Kelly, K.E., Whitaker, J., Petty, A., Widmer, C., Dybwad, A., Sleeth, D., Martin, R., Butterfield, A., 2017. Ambient and laboratory evaluation of a low-cost particulate matter sensor. Environ. Pollut. 221, 491–500. https://doi.org/10.1016/j.envpol.2016.12.039.
Kiss, G., Imre, K., Molnar, A., Gelencser, A., 2017. Bias caused by water adsorption in hourly PM measurements. Atmos. Meas. Tech. 10, 2477–2484. https://doi.org/10.5194/amt-10-2477-2017.
Koehler, K., Latshaw, M., Matte, T., Kass, D., Frumkin, H., Fox, M., Hobbs, B.F., Wills-Karp, M., Burke, T.A., 2018. Building healthy community environments: a public health approach. Publ. Health Rep. 133, 35S–43S. https://doi.org/10.1177/0033354918798809.
Kovacs, M., Călămar, A.-N., Toth, L., Simion, S., Simion, A., 2021. Comparative measurements between the results achieved with reference method and the optical method for determination of PM_{10} dusts in ambient air. MATEC Web of Conf. 342, 03002. https://doi.org/10.1051/matecconf/202134203002.
Kulkarni, P.S., Bortoli, D., Silva, A.M., 2013. Nocturnal surface ozone enhancement and trend over urban and suburban sites in Portugal. Atmos. Environ. 71, 251–259. https://doi.org/10.1016/j.atmosenv.2013.01.051.
Kulkarni, P.S., Dasari, H.P., Sharma, A., Bortoli, D., Salgado, R., Silva, A.M., 2016. Nocturnal surface ozone enhancement over Portugal during winter: influence of different atmospheric conditions. Atmos. Environ. 147, 109–120. https://doi.org/10.1016/j.atmosenv.2016.09.056.
Lee, J.-Y., Marotzke, J., Bala, G., Cao, L., Corti, S., Dunne, J.P., Engelbrecht, F., Fischer, E., Fyfe, J.C., Jones, C., Maycock, A., Mutemi, J., Ndiaye, O., Panickal, S., Zhou, T., 2021. Future global climate: scenario-based projections and near-term information. In: Climate Change 2021: the Physical Science Basis. Contribution of Working Group I to the Sixth Assessment Report of the. Intergovernmental Panel on Climate Change, pp. 553–672. https://doi.org/10.1017/9781009157896.006.553.
Lelieveld, J., Evans, J.S., Fnais, M., Giannadaki, D., Pozzer, A., 2015. The contribution of outdoor air pollution sources to premature mortality on a global scale. Nature 525, 367–371. https://doi.org/10.1038/nature15371.
Li, H., Wu, J., Wang, A., Li, X., Chen, S., Wang, T., Amsalu, E., Gao, Q., Luo, Y., Yang, X., Wang, W., Guo, J., Guo, Y., Guo, X., 2018. Effects of ambient carbon monoxide on daily hospitalizations for cardiovascular disease: a time-stratified case-crossover study of 460,938 cases in Beijing, China from 2013 to 2017. Environ. Health 17, 82. https://doi.org/10.1186/s12940-018-0429-3.
Liang, L., 2021. Calibrating low-cost sensors for ambient air monitoring: techniques, trends, and challenges. Environ. Res. https://doi.org/10.1016/j.envres.2021.111163.
Liu, C., Chen, R., Sera, F., Vicedo-Cabrera, A.M., Guo, Y., Tong, S., Coelho, M.S.Z.S., Saldiva, P.H.N., Lavigne, E., Matus, P., Valdes Ortega, N., Osorio Garcia, S., Pascal, M., Stafoggia, M., Scortichini, M., Hashizume, M., Honda, Y., Hurtado-Díaz, M., Cruz, J., Nunes, B., Teixeira, J.P., Kim, H., Tobias, A., Íñiguez, C., Forsberg, B., Åström, C., Ragettli, M.S., Guo, Y.-L., Chen, B.-Y., Bell, M.L., Wright, C. Y., Scovronick, N., Garland, R.M., Milojevic, A., Kyselý, J., Urban, A., Orru, H., Indermitte, E., Jaakkola, J.J.K., Ryti, N.R.I., Katsouyanni, K., Analitis, A., Zanobetti, A., Schwartz, J., Chen, J., Wu, T., Cohen, A., Gasparrini, A., Kan, H., 2019. Ambient particulate air pollution and daily mortality in 652 cities. N. Engl. J. Med. 381, 705–715. https://doi.org/10.1056/nejmoa1817364.
Liu, C., Henderson, B.H., Wang, D., Yang, X., Peng, Z.R., 2016. A land use regression application into assessing spatial variation of intra-urban fine particulate matter ($PM_{2.5}$) and nitrogen dioxide (NO_2) concentrations in city of Shanghai. China. Sci. Total Environ. 565, 607–615. https://doi.org/10.1016/j.scitotenv.2016.03.189.
Liu, H., Pei, X., Zhang, F., Song, Y., Kuang, B., Xu, Z., Wang, Z., 2023. Relative humidity dependence of growth factor and real refractive index for sea salt/malonic acid internally mixed aerosols. J. Geophys. Res. Atmos. 128. https://doi.org/10.1029/2022JD037579.
Liu, H., Tian, Y., Xiang, X., Li, M., Wu, Y., Cao, Y., Juan, J., Song, J., Wu, T., Hu, Y., 2018. Association of short-term exposure to ambient carbon monoxide with hospital admissions in China. Sci. Rep. 8, 13336. https://doi.org/10.1038/s41598-018-31434-1.
Lopes, M., Reis, J., Fernandes, A.P., Lopes, D., Lourenço, R., Nunes, T., Faria, C.H.G., Borrego, C., Miranda, A.I., 2020. Indoor air quality study using low-cost sensors. WIT Trans. Ecol. Environ. 244, 1–13. https://doi.org/10.2495/AIR200011.
Ma, Z., Hu, X., Huang, L., Bi, J., Liu, Y., 2014. Estimating ground-level $PM_{2.5}$ in China using satellite remote sensing. Environ. Sci. Technol. 48, 7436–7444. https://doi.org/10.1021/es5009399.
Magi, B., Cupini, C., Francis, J., Green, M., Hauser, C., 2020. Evaluation of PM2.5 measured in an urban setting using a low-cost optical particle counter and a federal equivalent method beta attenuation monitor. Aerosol Sci. Technol. 54, 147–159. https://doi.org/10.1080/02786826.2019.1619915.
Malings, C., Westervelt, D.M., Hauryliuk, A., Presto, A.A., Grieshop, A., Bittner, A., Beekmann, M., Subramanian, R., 2020. Application of low-cost fine particulate mass monitors to convert satellite aerosol optical depth to surface concentrations in North America and Africa. Atmos. Meas. Tech. 13, 3873–3892. https://doi.org/10.5194/amt-13-3873-2020.
Mandal, J., Samanta, S., Chanda, A., Halder, S., 2021. Effects of COVID-19 pandemic on the air quality of three megacities in India. Atmos. Res. 259, 105659. https://doi.org/10.1016/j.atmosres.2021.105659.
McFarlane, C., Isevulambire, P.K., Lumbuenamo, R.S., Ndinga, A.M.E., Dhammapala, R., Jin, X., McNeill, V.F., Malings, C., Subramanian, R., Westervelt, D.M., 2021. First measurements of ambient $PM_{2.5}$ in Kinshasa, Democratic Republic of Congo and Brazzaville, Republic of Congo using field-calibrated low-cost sensors. Aerosol Air Qual. Res. 21, 200619. https://doi.org/10.4209/aaqr.200619.
Mei, H., Wang, L., Wang, M., Zhu, R., Wang, Y., Li, Y., Zhang, R., Wang, B., Bao, X., 2021. Characterization of exhaust CO, HC and NOx emissions from light-duty vehicles under real driving conditions. Atmosphere 12, 1125. https://doi.org/10.3390/atmos12091125.
Mishra, M., Kulshrestha, U.C., 2021. A brief review on changes in air pollution scenario over South Asia during COVID-19 lockdown. Aerosol Air Qual. Res. 21, 200541. https://doi.org/10.4209/aaqr.200541.
Moreira, G. de A., Cacheffo, A., Andrade, I. da S., Lopes, F.J. da S., Gomes, A.A., Landulfo, E., 2023. Analyzing the influence of vehicular traffic on the concentration of pollutants in the city of São Paulo: an approach based on pandemic SARS-CoV-2 data and deep learning. Atmosphere 14, 1578. https://doi.org/10.3390/atmos14101578.
Makoni, Munyaradzi, 2020. Air pollution in Africa. Lancet Respir. Med. 8, 60–61. https://doi.org/10.1016/S2213-2600(20)30275-7.
Nakata, M., Sano, I., Mukai, S., 2015. Air pollutants in Osaka (Japan). Front. Environ. Sci. 3, 18. https://doi.org/10.3389/fenvs.2015.00018.
Nguyen, G.T.H., La, L.T., Hoang-Cong, H., Le, A.H., 2024. An exploration of meteorological effects on $PM_{2.5}$ air quality in several provinces and cities in Vietnam. J. Environ. Sci. 145, 139–151. https://doi.org/10.1016/j.jes.2023.07.020.
Niemenmaa, V., Happach, B., Kubat, J., Otto, J., Pirelli, L., Simeonova, R., Zalega, A., Wisniewska-Danek, K., Radecka-Moroz, K., Wojciechowski, J., Soblet, F., Friel, C., Coelho, J., 2018. Special Report: Air Pollution: Our Health Still Insufficiently Protected. Publications Office of the European Union, Luxembourg. https://doi.org/10.2865/46457.
Njalsson, T., Novosselov, I., 2018. Design and optimization of a compact low-cost optical particle sizer. J. Aerosol Sci. 119, 1–12. https://doi.org/10.1016/j.jaerosci.2018.01.003.
Nogueira, T., Kamigauti, L.Y., Pereira, G.M., Gavidia-Calderón, M.E., Ibarra-Espinosa, S., De Oliveira, G.L., De Miranda, R.M., De Castro Vasconcellos, P.D., de Freitas, E.D., De Fatima Andrade, M., 2021. Evolution of vehicle emission factors in a megacity affected by extensive biofuel use: results of tunnel measurements in São Paulo, Brazil. Environ. Sci. Technol. 55, 6677–6687. https://doi.org/10.1021/acs.est.1c01006.
Nurowska, K., Markowicz, K., 2023. Determination of hygroscopic aerosol growth based on the OPC-N3 counter. Atmosphere 15 (1), 61. https://doi.org/10.3390/atmos15010061.
O'Brien, R.M., 2007. A caution regarding rules of thumb for variance inflation factors. Qual. Quantity 41, 673–690. https://doi.org/10.1007/s11135-006-9018-6.
Pinder, R.W., Klopp, J.M., Kleiman, G., Hagler, G.S.W., Awe, Y., Terry, S., 2019. Opportunities and challenges for filling the air quality data gap in low- and middle-income countries. Atmos. Environ. 215, 1–11. https://doi.org/10.1016/j.atmosenv.2019.06.032.
Qiu, J., He, B., Zhang, L., Cheng, M., Guo, S., Fan, C., Zhao, C., 2024. Hygroscopic behavior of sea spray aerosols in offshore waters and open sea areas investigated with aerosol optical tweezers. Atmos. Environ. https://doi.org/10.1016/j.atmosenv.2024.120360.
Raheja, G., Balmes, J.R., Gould, T., Malings, C., Subramanian, R., Presto, A.A., 2023. Low-cost sensor performance intercomparison, correction, and implications for monitoring in regions with limited reference infrastructure. Environ. Sci. Technol. 57 (13), 4995–5006. https://doi.org/10.1021/acs.est.2c09264.
Rees, N., Wickham, A., Choi, Y., 2019. Silent suffocation in Africa air pollution is a growing menace. Affecting the Poorest Children the Most. UNICEF, New York.
Reich, O., Gleichweit, M.J., David, G., Leemann, N., Signorell, R., 2023. Hygroscopic growth of single atmospheric sea salt aerosol particles from mass measurement in an optical trap. Environ. Sci.: Atmos. 3, 695–707. https://doi.org/10.1039/d2ea00129b.
Rosenthal, N.A., 2015. Infections, chronic disease, and the epidemiological transition: a new perspective. Clin. Infect. Dis. 61, 489–490. https://doi.org/10.1093/cid/civ280.
Rozante, J.R., Rozante, V., Alvim, D.S., Manzi, A.O., Chiquetto, J.B., D'Amelio, M.T.S., Moreira, D.S., 2017. Variations of carbon monoxide concentrations in the megacity of São Paulo from 2000 to 2015 in different time scales. Atmosphere 8, 81. https://doi.org/10.3390/atmos8050081.
Sá, J., Chojer, H., Branco, P., Alvim-Ferraz, M., Martins, F.G., Sousa, S., 2022. Two-step calibration method for ozone low-cost sensor: field experiences with the UrbanSense DCUs. J. Environ. Manag. 328, 116910. https://doi.org/10.1016/j.jenvman.2022.116910.
Samad, A., Nuñez, D.R.O., Castillo, G.C.S., Laquai, B., Vogt, U., 2020. Effect of relative humidity and air temperature on the results obtained from low-cost gas sensors for

ambient air quality measurements. Sensors 20, 1–29. https://doi.org/10.3390/s20185175.
Seltenrich, N., 2017. A satellite–ground hybrid approach: relative risks for exposures to $PM_{2.5}$ estimated from a combination of data sources. Environ. Health Perspect. https://doi.org/10.1289/EHP.125-A73.
Shikwambana, L., Tsoeleng, L.T., 2020. Impacts of population growth and land use on air quality. A case study of Tshwane, Rustenburg and Emalahleni, South Africa. S. Afr. Geogr. J. 102, 209–222. https://doi.org/10.1080/03736245.2019.1670234.
Simwela, A., Xu, B., Mekondjo, S.S., Morie, S., 2018. Air quality concerns in Africa: a literature review. Int. J. Sci. Res. Publ. 8, 588–594. https://doi.org/10.29322/ijsrp.8.5.2018.p7776.
Song, C., Wu, L., Xie, Y., He, J., Chen, X., Wang, T., Lin, Y., Jin, T., Wang, A., Liu, Y., Dai, Q., Liu, B., Wang, Y. nan, Mao, H., 2017. Air pollution in China: status and spatiotemporal variations. Environ. Pollut. 227, 334–347. https://doi.org/10.1016/j.envpol.2017.04.075.
Spinelle, L., Gerboles, M., Villani, M.G., Aleixandre, M., Bonavitacola, F., 2017. Field calibration of a cluster of low-cost commercially available sensors for air quality monitoring. Part B: NO, CO and CO_2. Sensor. Actuator. B Chem. 238, 706–715. https://doi.org/10.1016/j.snb.2016.07.036.
Spinelle, L., Gerboles, M., Villani, M.G., Aleixandre, M., Bonavitacola, F., 2015. Field calibration of a cluster of low-cost available sensors for air quality monitoring. Part A: ozone and nitrogen dioxide. Sensor. Actuator. B Chem. 215, 249–257. https://doi.org/10.1016/j.snb.2015.03.031.
Subramanian, R., Beekmann, M., Malings, C., Presto, A.A., 2024. Filling the air quality data gap in Africa using lower-cost monitors. GeoHealth 8 (6), e2024GH001049. https://doi.org/10.1029/2024GH001049.
Tamura, R., Kobayashi, K., Takano, Y., Miyashiro, R., Nakata, K., Matsui, T., 2018. Mixed integer quadratic optimisation formulations for eliminating multicollinearity based on variance inflation factor. J. Global Optim. 73, 431–446. https://doi.org/10.1007/s10898-018-0713-3.
Tan, W., Wang, Haolin, Su, J., Sun, R., He, C., Lu, X., Lin, J., Xue, C., Wang, Haichao, Liu, Y., Liu, L., Zhang, L., Wu, D., Mu, Y., Fan, S., 2023. Soil emissions of reactive nitrogen accelerate summertime surface ozone increases in the North China Plain. Environ. Sci. Technol. 57, 12782–12793. https://doi.org/10.1021/acs.est.3c01823.
Triantafyllou, E., Diapouli, E., Tsilibari, E.M., Adamopoulos, A.D., Biskos, G., Eleftheriadis, K., 2016. Assessment of factors influencing PM mass concentration measured by gravimetric & beta attenuation techniques at a suburban site. Atmos. Environ. 131, 409–417. https://doi.org/10.1016/j.atmosenv.2016.02.010.
Tyagi, S., Tiwari, S., Mishra, A., Hopke, P.K., Attri, S.D., Srivastava, A.K., Bisht, D.S., 2016. Spatial variability of concentrations of gaseous pollutants across the National Capital Region of Delhi, India. Atmos. Pollut. Res. 7, 808–816. https://doi.org/10.1016/j.apr.2016.04.008.
U.S. EPA, 2014. National Ambient Air Quality Standards (NAAQS). United States Environmental Protection Agency, Washington, D.C.
Vanesa, V., Guerrero, U., Vinicius Bueno De Morais, M., Dias De Freitas, E., Martins, L.D., 2021. Numerical study of meteorological factors for tropospheric nocturnal ozone increase in the metropolitan area of São Paulo. Atmosphere 12, 287. https://doi.org/10.3390/atmos12020287.
Wang, G., Yu, C., Guo, K., Guo, H., Wang, Y., 2024. Research of low-cost air quality monitoring models with different machine learning algorithms. Atmos. Meas. Tech. 17, 181–199. https://doi.org/10.5194/amt-17-181-2024.
Wang, T., Xue, L., Brimblecombe, P., Lam, Y.F., Li, L., Zhang, L., 2017. Ozone pollution in China: a review of concentrations, meteorological influences, chemical precursors, and effects. Sci. Total Environ. 575, 1582–1596. https://doi.org/10.1016/j.scitotenv.2016.10.081.
WHO, 2021. WHO global air quality guidelines: particulate matter ($PM_{2.5}$ and PM_{10}), ozone, nitrogen dioxide. Sulfur Dioxide and Carbon Monoxide. World Health Organization, Switzerland.
Xie, M., Zhu, K., Wang, T., Chen, P., Han, Y., Li, S., Zhuang, B., Shu, L., 2016. Temporal characterization and regional contribution to O_3 and NOx at an urban and a suburban site in Nanjing. China. Sci. Total Environ. 551–552, 533–545. https://doi.org/10.1016/j.scitotenv.2016.02.047.
Yang, Z., Yang, J., Li, M., Chen, J., Ou, C.Q., 2021. Nonlinear and lagged meteorological effects on daily levels of ambient $PM_{2.5}$ and O_3: evidence from 284 Chinese cities. J. Clean. Prod. 278, 123931. https://doi.org/10.1016/j.jclepro.2020.123931.
Yoshino, A., Takami, A., Hara, K., Nishita-Hara, C., Hayashi, M., Kaneyasu, N., 2021. Contribution of local and transboundary air pollution to the urban air quality of Fukuoka, Japan. Atmosphere 12, 431. https://doi.org/10.3390/atmos12040431.
Zafra-Pérez, A., Boente, C., de la Campa, A.S., Gómez-Galán, J.A., de la Rosa, J.D., 2022. A novel application of mobile low-cost sensors for atmospheric particulate matter monitoring in open-pit mines. Environ. Technol. Innov. 29, 102974. https://doi.org/10.1016/j.eti.2022.102974.
Zhang, D., Du, L., Wang, W., Zhu, Q., Bi, J., Scovronick, N., Naidoo, M., Garland, R.M., Liu, Y., 2021. A machine learning model to estimate ambient $PM_{2.5}$ concentrations in industrialized highveld region of South Africa. Remote Sens. Environ. 266, 112713. https://doi.org/10.1016/j.rse.2021.112713.
Zheng, T., Bergin, M.H., Johnson, K.K., Tripathi, S.N., Shirodkar, S., Landis, M.S., Sutaria, R., Carlson, D.E., 2018. Field evaluation of low-cost particulate matter sensors in high-and low-concentration environments. Atmos. Meas. Tech. 11, 4823–4846. https://doi.org/10.5194/amt-11-4823-2018.
Ziemke, J.R., Strode, S.A., Douglass, A.R., Joiner, J., Vasilkov, A., Oman, L.D., Liu, J., Strahan, S.E., Bhartia, P.K., Haffner, D.P., 2017. A cloud-ozone data product from Aura OMI and MLS satellite measurements. Atmos. Meas. Tech. 10, 4067–4078. https://doi.org/10.5194/amt-10-4067-2017.
Zikova, N., Hopke, P.K., Ferro, A.R., 2017. Evaluation of new low-cost particle monitors for $PM_{2.5}$ concentrations measurements. J. Aerosol Sci. 105, 24–34. https://doi.org/10.1016/j.jaerosci.2016.11.010.
Zou, S., Chen, L., Xu, H., Zhang, R., Liu, M., Liu, G., Ye, J., Yang, H., Wu, H., Yang, Y., Zhang, F., 2024.
Zusman, M., Schumacher, C.S., Gassett, A.J., Spalt, E.W., Austin, E., Larson, T.V., Carvlin, G., Seto, E., Kaufman, J.D., Sheppard, L., 2020. Calibration of low-cost particulate matter sensors: model development for a multi-city epidemiological study. Environ. Int. 134. https://doi.org/10.1016/j.envint.2019.105329.